Project Report
NASA/L-3

Aircraft Vortex Spacing System (AVOSS) Initial 1997 System Deployment at Dallas/Ft. Worth (DFW) Airport

T.J. Dasey
R.E. Cole
R.M. Heinrichs
M.P. Matthews
G.H. Perras

8 July 1998

Lincoln Laboratory
MASSACHUSETTS INSTITUTE OF TECHNOLOGY
LEXINGTON, MASSACHUSETTS

Prepared for the National Aeronautics and Space Administration
Langley Research Center, Hampton, Virginia 23680-2199.

This document is available to the public through
the National Technical Information Service,
Springfield, Virginia 22161.

3 August, 1998

ERRATA

Document: Project Report NASA/L-3
Aircraft Vortex Spacing System (AVOSS)
Initial 1997 System Deployment at Dallas/Ft. Worth (DFW) Airport
8 July 1998

Corrections have been made to pages 56 and 61. The corrected pages, attached, are provided for you to insert into your copy of this document.

Publications Office
MIT Lincoln Laboratory
244 Wood St.
Lexington, MA 02420-9108

for the SAVPAK locations. All data are one–minute averages output every minute. The SAVPAK data format is shown in Table A–6.

The FLUXPAK data files consist of the covariance measurements at the sonic anemometer locations on the instrumented towers. The sensors directly measure the east–west and north–south wind component as well as the virtual temperature. All measurements are performed at a 10Hz data rate, averaged for one minute and output every minute. The format for the FLUXPAK data are shown in Table A–7.

The Soil data files consist of the soil measurements performed at both the north and south meteorological sites. The sensors' output included in this data file are the Soil Temperature Probe (STP–1), the Soil Moisture Probe (SMP–1), the Rain Gauge (TE525), and the Total Hemispherical Radiometer (THRDS–7). The Soil Temperature Probe and the Soil Moisture Probe are located at the depth indicated in the file. The Rain Gauge and Radiometer are mounted on an aluminium structure at a two–meter height. All data are one–minute averages output every minute. The Soil data file format is shown in Table A–8.

The Doppler Profile Analysis (DPA) files contain wind profile information derived from TDWR data. A file is created for each GMT calendar day for each TDWR radar and is separated internally into five–minute blocks. Each block contains a commented header (comment lines are denoted by a # symbol as the first character). Each header is followed by the actual wind data provided by the DPA algorithm. The DPA file format is shown in Table A–9 and Table A–10.

The wind profile data files contain U and V component wind information provided by the AVOSS Wind Analysis System (AWAS). A file is created for each GMT calendar day and is separated internally by five–minute blocks. Each block contains a commented header (comment lines are denoted by a # symbol as the first character). Each header is followed by the actual headwind and crosswind data. The AWAS file format is shown in Table A–11 and Table A–12.

Table A–12.
AWAS Data File Contents

	Variable	Units	Description
1	Height	meters AGL	Height at which values are interpolated
2	U component	m/s	West to East wind
3	V component	m/s	South to North wind
4	U component variance	m/s	Goodness of fit for U component
5	V component variance	m/s	Goodness of fit for V component
6	U component spatial variability	m/s	Crosswind average of all current sensor variability readings in U component
7	V component spatial variability	m/s	Headwind average of all current sensor variability readings in V component
8	U component temporal variability	m/s	Crosswind average of all past U component sensor variability readings
9	V component temporal variability	m/s	Headwind average of all past V component sensor variability readings
10	U component vertical shear	m/s / m	Change in U component values with height

TECHNICAL REPORT STANDARD TITLE PAGE

1. Report No.	2. Government Accession No.	3. Recipient's Catalog No.
NASA/L-3		

4. Title and Subtitle	5. Report Date
Aircraft Vortex Spacing System (AVOSS) Initial 1997 System Deployment at Dallas/Ft. Worth (DFW) Airport	8 July 1998
	6. Performing Organization Code
7. Author(s)	8. Performing Organization Report No.
T.J. Dasey, R.E. Cole, R.M. Heinrichs, M.P. Matthews, and G.H. Perras	NASA/L-3
9. Performing Organization Name and Address	10. Work Unit No. (TRAIS)
MIT Lincoln Laboratory 244 Wood Street Lexington, MA 02420-9108	11. Contract or Grant No. NASA Langley
12. Sponsoring Agency Name and Address	13. Type of Report and Period Covered
National Aeronautics and Space Administration Langley Research Center Hampton, VA 23680-2199	Project Report
	14. Sponsoring Agency Code

15. Supplementary Notes

This report is based on studies performed at Lincoln Laboratory, a center for research operated by Massachusetts Institute of Technology, under Contract to NASA Langley Research Center.

16. Abstract

The potential hazard of aircraft encounters with the wake turbulence of preceding aircraft requires the use of minimum separations on landing that are a significant constraint on airport arrival capacity during instrument flight rules (IFR) conditions. The National Aeronautics and Space Administration (NASA) Langley Research Center has been researching the development of the Aircraft Vortex Spacing System (AVOSS) which would dynamically change aircraft arrival separations based on the forecasted weather conditions and vortex behavior.

An experimental AVOSS test system has been constructed at DFW airport and includes a large set of meteorological instruments, wake vortex sensors from three organizations, and an aircraft data collection system. All of this data are relayed to a central processing center at DFW for processing by automated meteorological data fusion algorithms and by NASA vortex behavior predictions software. An initial deployment and test of the DFW system was conducted during a three-week period in September/October of 1997. This document describes the overall system, the Lincoln-deployed sensors, including the Continuous-Wave Coherent lidar, and the meteorological data collection and processing system. Algorithms that were used to process the data for scientific use are described, as well as the conditions of the data collection and the data formats, for potential users of this database.

17. Key Words			18. Distribution Statement
wake	vortex	DFW	This document is available to the public through the National Technical Information Service, Springfield, VA 22161.
AVOSS	lidar	weather	

19. Security Classif. (of this report)	20. Security Classif. (of this page)	21. No. of Pages	22. Price
Unclassified	Unclassified	84	

ABSTRACT

The potential hazard of aircraft encounters with the wake turbulence of preceding aircraft requires the use of minimum separations on landing that are a significant constraint on airport arrival capacity during instrument flight rules (IFR) conditions. The National Aeronautics and Space Administration (NASA) Langley Research Center has been researching the development of the Aircraft Vortex Spacing System (AVOSS) which would dynamically change aircraft arrival separations based on the forecasted weather conditions and vortex behavior.

An experimental AVOSS test system has been constructed at DFW airport and includes a large set of meteorological instruments, wake vortex sensors from three organizations, and an aircraft data collection system. All of this data are relayed to a central processing center at DFW for processing by automated meteorological data fusion algorithms and by NASA vortex behavior prediction software. An initial deployment and test of the DFW system was conducted during a three–week period in September/October of 1997. This document describes the overall system, the Lincoln–deployed sensors, including the Continuous–Wave Coherent lidar, and the meteorological data collection and processing system. Algorithms that were used to process the data for scientific use are described, as well as the conditions of the data collection and the data formats, for potential users of this database.

ACKNOWLEDGMENTS

The authors thank the many individuals who worked so hard to put the DFW wake vortex system together and operate it in a successful deployment. Efforts like this require the enthusiasm and cooperation of many organizations, long hours, and a little faith, on occasion. We especially thank the entire Lincoln project team who worked very hard to put the DFW system together and to ensure a successful deployment: Charlie Cobbett, Skip Copeland, Mo Couture, Andy Denneno, Duane Grant, Ralph Halvorsen, Rose Joseph, Steve Marcus, Pat Pawlak, Doug Piercey, Kim Theriault and Dave Tremblay. The Lincoln DFW site team of Brad Crowe, Dave Miller, Dale Rhoda and Tim Rotz were very enthusiastic about the project and dealt admirably with all of the distractions and details that the deployment posed. David Hinton, Donner Grigsby and Richard Walters of NASA Langley, Al Zak of Vigyan, Inc., and Bob Rudis of the Volpe Transportation Systems Center were instrumental in providing leadership and guidance for this work. We thank Al Zak for his assistance in characterizing the meteorological conditions for this document. Numerous people with the DFW airport, led by Jim Crites, provided the perfect environment where this research and development could be performed. In particular, we thank the efforts of Kathy Houk, Al Magazzine, Curtis Inglis, Craig Miller, Mike Pyles, Rick Paddock, Noresh Shahanni and Mike Sympson. We thank the DFW tower and TRACON personnel who were very cooperative in allowing us to launch weather balloons from airport property. A special thanks to Captain David Strand and Rob Blume of American Airlines for graciously providing the project with landing weight information on their aircraft.

TABLE OF CONTENTS

TABLE OF CONTENTS
(Continued)

LIST OF ILLUSTRATIONS

LIST OF TABLES

1. INTRODUCTION

1.1. Background

The potential hazard of aircraft encounters with the wake turbulence of preceding aircraft has caused the Federal Aviation Administration (FAA) to designate minimum separation distances behind leading aircraft during final approach to a runway (Thompson, 1997). These separations are enforced by air traffic controllers during Instrument Flight Rules (IFR) and are a significant constraint on airport arrival capacity during these conditions. The behavior of wakes is highly dependant on the local weather conditions, and there is reason to believe that in most situations the FAA–mandated separations are overly conservative.

The National Aeronautics and Space Administration (NASA) Langley Research Center, in cooperation with the FAA, has been researching the development of a system which could dynamically change aircraft arrival separations based on the forecasted weather conditions (Hinton, 1995). This system, coined the Aircraft Vortex Spacing System (AVOSS), has been under research since 1994. As part of this effort, Lincoln Laboratory constructed a mobile continuous–wave coherent CO_2 lidar for the observation and tracking of wake vortices (Heinrichs, et al., 1995). An extensive meteorological data collection and processing system was installed at Memphis International Airport and operated from 1994 to 1997 (Dasey, et al., 1997; Matthews, et al., 1997; Campbell, et al., 1997; Campbell, et al., 1996; Campbell, et al., 1995). The CO_2 lidar was used to make vortex measurements at Memphis Airport (MEM) during two one–month deployments. The database of weather and vortex observations from Memphis has been made available by NASA to selected parties, and the complete Memphis system and dataset has been documented in a manner similar to this report (Campbell, et al., 1997).

1.2. DFW Deployment

In February, 1997 the Memphis meteorological data collection site was dismantled and moved to Dallas/Ft. Worth (DFW) Airport. Construction on DFW meteorological sites was completed in July of the same year. The reasons for moving to DFW included the presence of both Integrated Terminal Weather System (ITWS) (Evans and Ducot, 1994) and Center/TRACON Automation System (CTAS) (Denery and Erzberger, 1995) test sites (both of which may interface to an eventual AVOSS) and the higher traffic density of DFW.

An initial field deployment, which included the use of the Lincoln CW lidar vortex sensor as well as a NASA pulsed 2 μm lidar and an anemometer array (termed a windline) operated by the Volpe Transportation System Center, was held in September and October of 1997. This document describes that deployment, including the setup, the instruments used by Lincoln Laboratory, and the data generated by those instruments.

Much of the software and hardware used in this 1997 DFW deployment had been newly introduced into the DFW AVOSS setup, and interfaces between algorithms and sensors had only recently been established. As a result, the goals of this deployment were, in order of priority:

- Operate and test AVOSS operation in a real–time mode. Establish all required AVOSS subsystems and interfaces required for real–time operation.

- Collect atmospheric data and demonstrate the ability to provide real–time quality screening, sensor data integration, and statistical profiles of variables relevant to vortex transport and decay (wind, temperature and turbulence).
- Collect data which can help identify the critical modes (transport or decay) and critical approach windows for airport capacity improvement in the DFW environment.
- Implement software and hardware suitable for year–round AVOSS operation.
- Gather additional wake vortex behavior data for weather regimes and aircraft types not observed at Memphis. Gather large scale atmospheric data for Planetary Boundary Layer (PBL) simulation validations.

The deployment took place over approximately a three–week period, as is shown in Figure 1. Several organizations collaborated to launch weather balloons at six locations at and around DFW during the first two weeks of the deployment. The Lincoln and NASA lidars were operated during all three weeks. Weather conditions generally were very hot and humid, with light crosswinds. A few days during the second week had substantial periods of IFR conditions (due to low ceilings), and the Lincoln lidar was making measurements of vortices generated inside the threshold during this period. The Volpe Transportations System Center windline and all of the meteorological sensors were collecting data continuously over the entire period.

1.3. Organization of Report

This report describes the system setup, sensors and algorithms used at DFW during the 1997 Dallas/Ft. Worth (DFW) Airport Aircraft Vortex Spacing System (AVOSS) deployment. Section 2 describes the layout of sensors, computers and processing modules at DFW. Section 3 describes the Lincoln lidar sensor and the processing steps used to generated the lidar tracks, circulation estimates, and velocity profiles. Sections 4 and 5 provide similar details on the meteorological sensors and aircraft data, respectively. Section 6 gives a general synopsis of the vortex data collected and the weather conditions present during the deployment, and Section 7 summarizes the report. More detailed descriptions of data formats and sensor characteristics are described in Appendix. This report details the data collected and provided by Lincoln Laboratory. Additional information about data from other sensors, such as the NASA pulsed lidar and the Volpe anemometer array (windline) must be derived from other sources.

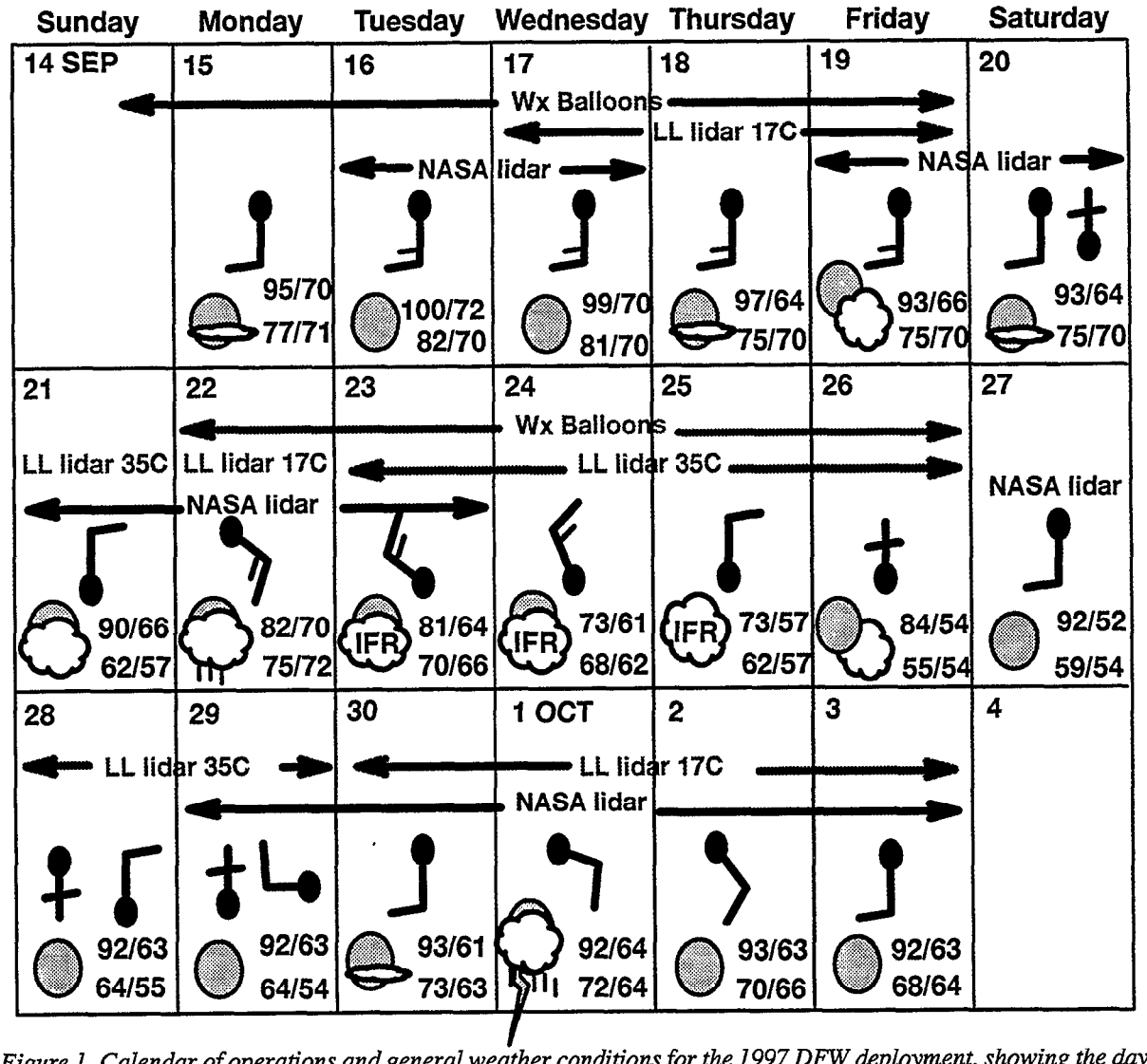

Figure 1. Calendar of operations and general weather conditions for the 1997 DFW deployment, showing the days of operations of the lidar systems, the days of weather balloon launches and general wind speed and direction (north is to the top of the page). The extent of cloud cover is shown, as well as the high temperature and dewpoint (upper numbers) and the low temperature and dewpoint at that time (lower numbers).

2. DFW AVOSS SYSTEM ORGANIZATION

2.1. Sensor Sites

The 1997 deployment at DFW used a number of sensors at a variety of locations around the airport. Figure 2 shows the layout at DFW and the placement of the various sensors. Wake measurements were focused on runway 17C/35C since this runway had a high arrival rate and provided favorable locations for siting the sensors. Meteorological measurements were made at two locations, one each at the north and south sides of the airport. Additional wind measurements were also obtained by the wake sensors. Data from all of the meteorological and wake sensors was sent in real time for processing to the Lincoln Laboratory office in the DFW Business Center. The Business Center is located in the center of the airport and is indicated by a solid–filled square in Figure 2.

Two lidars and a linear anemometer array (termed a windline) were used as wake sensors. The Lincoln Laboratory 10.6 μm Continuous–Wave (CW) lidar is a mobile unit and was deployed at four different locations (marked as lidar sites 17C007, 35C007, 35CIGE, and 17C008 in Figure 2) to make measurements of arrivals on 17C/35C during the deployment period. The Lincoln CW lidar is described in detail in Section 3 of this report. The NASA 2 μm pulsed lidar (deployed at lidar site "N" in the diagram) and the Volpe windline (marked by a dashed line) concentrated on arrival measurements on runway 17C and on departure measurements from runway 35C when those were possible.

The decision to construct two meteorological measurement sites at DFW was motivated by the desire to understand the spatial variability of the measurements and the expectation that the large terminal buildings located around the Business Center along the middle of the airport would alter the surface winds. Other than these buildings, the area around DFW is very homogeneous and flat. The predominant wind direction at DFW is from the south, so the highest concentration of in situ sensors located near the ground were placed at the south meteorological site where the wind was undisturbed by other ground obstacles. By similar reasoning, the majority of the time the aircraft land from the north. Therefore, most of the remote meteorological instruments were located at the north meteorological site so that they could make measurements at flight path altitudes closest to the actual aircraft locations. The meteorological sites, sensors, and processing algorithms are described in detail in Section 4 of this report.

2.2. Computer Network

One of the major goals of this deployment was to successfully demonstrate an integrated network of wake and meteorological sensors, processing computers, and interfaces with systems external to AVOSS. The data connections between these elements were designed to share real–time information.

As shown in Figure 3, the hub of the DFW wake vortex system was located in the DFW Business Center in the Lincoln Laboratory office. This office also houses the prototype Integrated Terminal Weather System (ITWS) and Center/TRACON Automation System (CTAS) networks. The presence of these systems at DFW was one of the major motivating factors for choosing DFW for the AVOSS work. Bidirectional network connections were established between each of the meteorological sites and the Business Center and between each of the wake sensors and the Business Center.

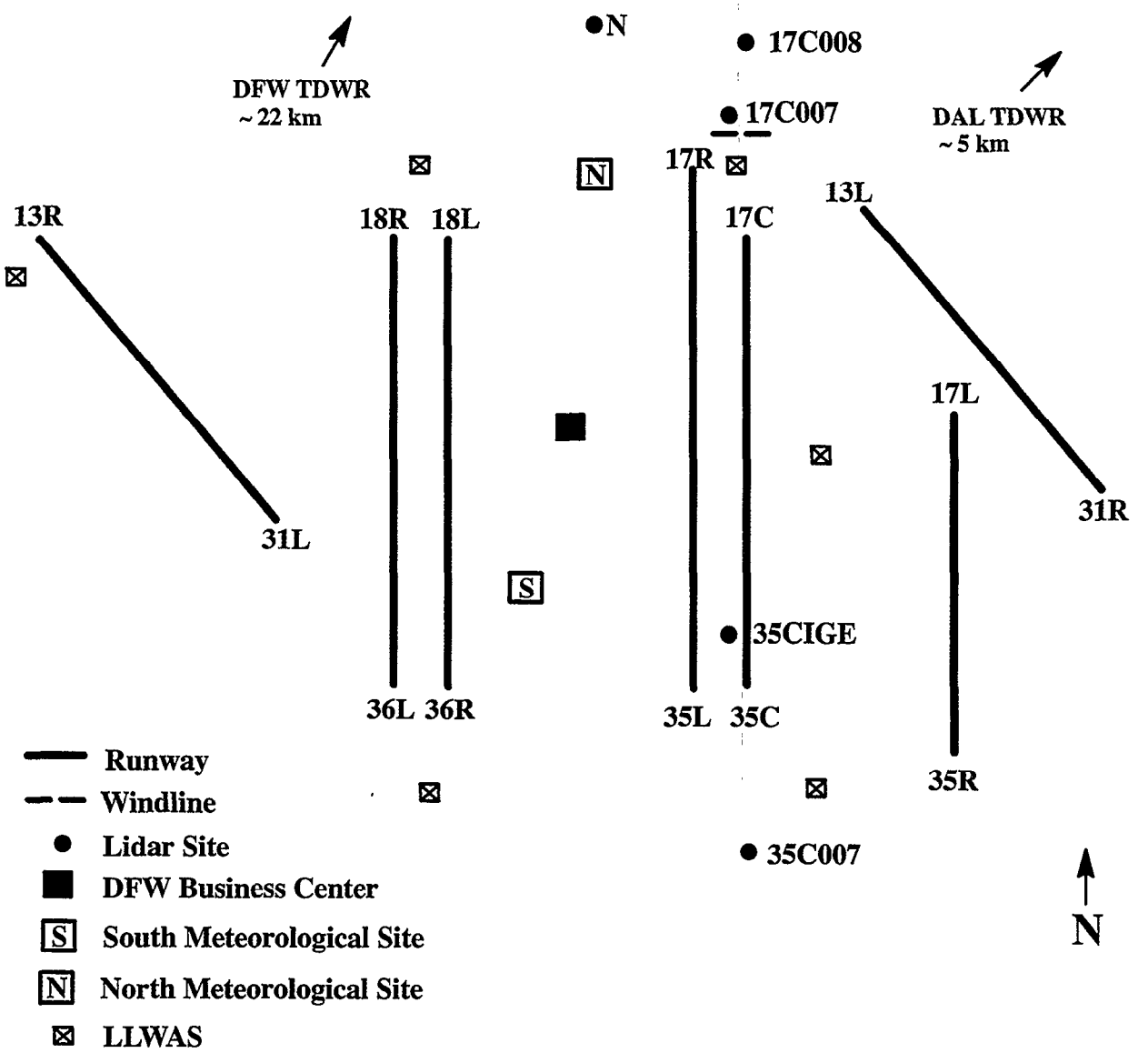

Figure 2. Schematic of the wake vortex sites at DFW during the 1997 deployment. The diagram is an overhead view of the airport.

All of the connections external to the Business Center were created using land phone lines, with the exception of the connection with the Lincoln lidar, which was a wireless link. To protect the integrity of the CTAS and ITWS systems, additional security measures were employed when interfacing with those systems. A connection was also established with computers at NASA Langley to facilitate remote maintenance and monitoring and to allow for the execution of the AVOSS behavior algorithm code and displays at Langley during non–deployment periods. A connection to the main Lincoln Laboratory facility in Lexington, Massachusetts is also used for maintenance and monitoring, as well as for software distribution and nightly data transfers to Lexington.

The functional organization and data flow used during this initial deployment is shown in Figure 4. The function of each of the data processing modules are described briefly in Table 1.

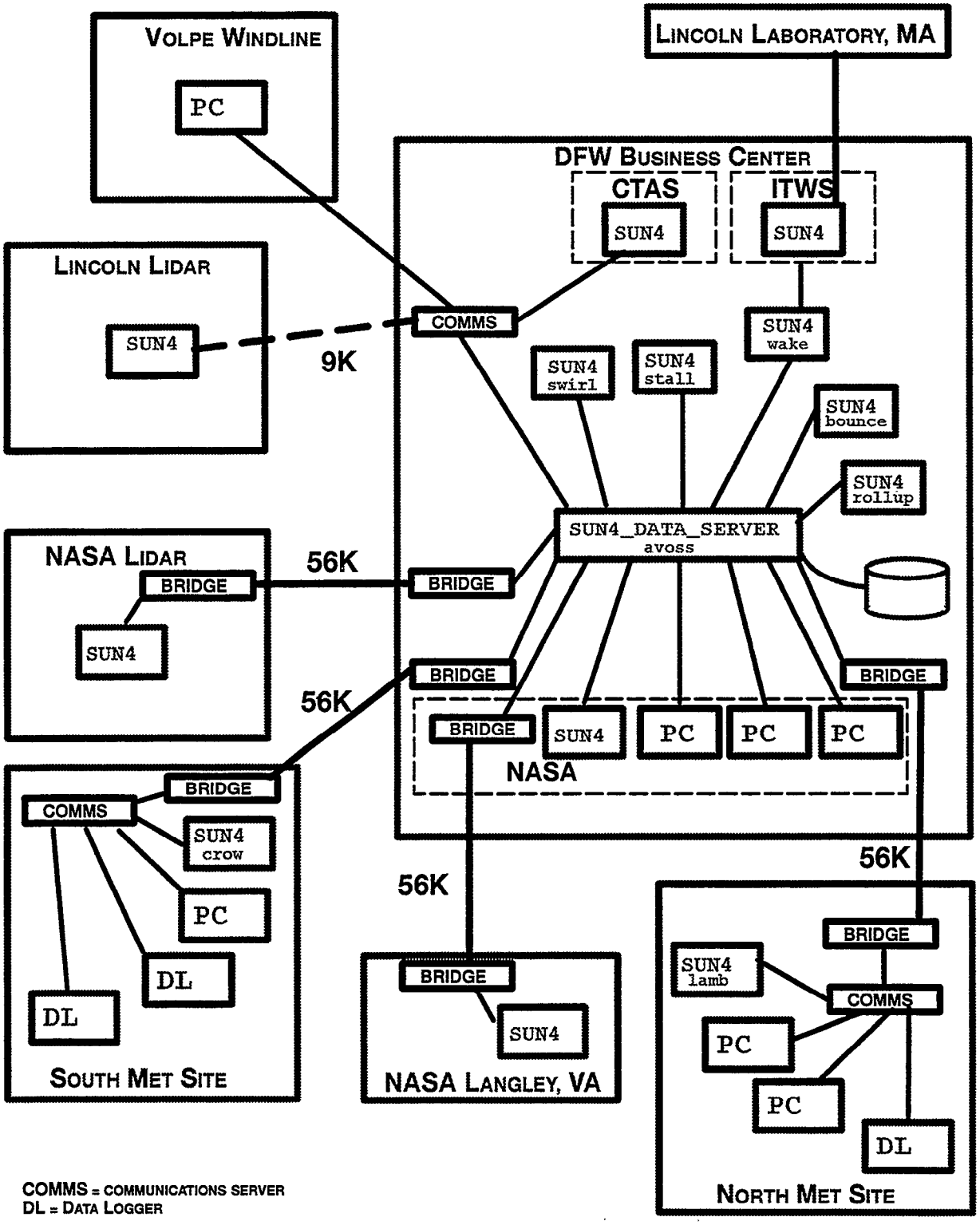

Figure 3. Diagram of the physical hardware arrangement and interfaces for the DFW Wake Vortex network.

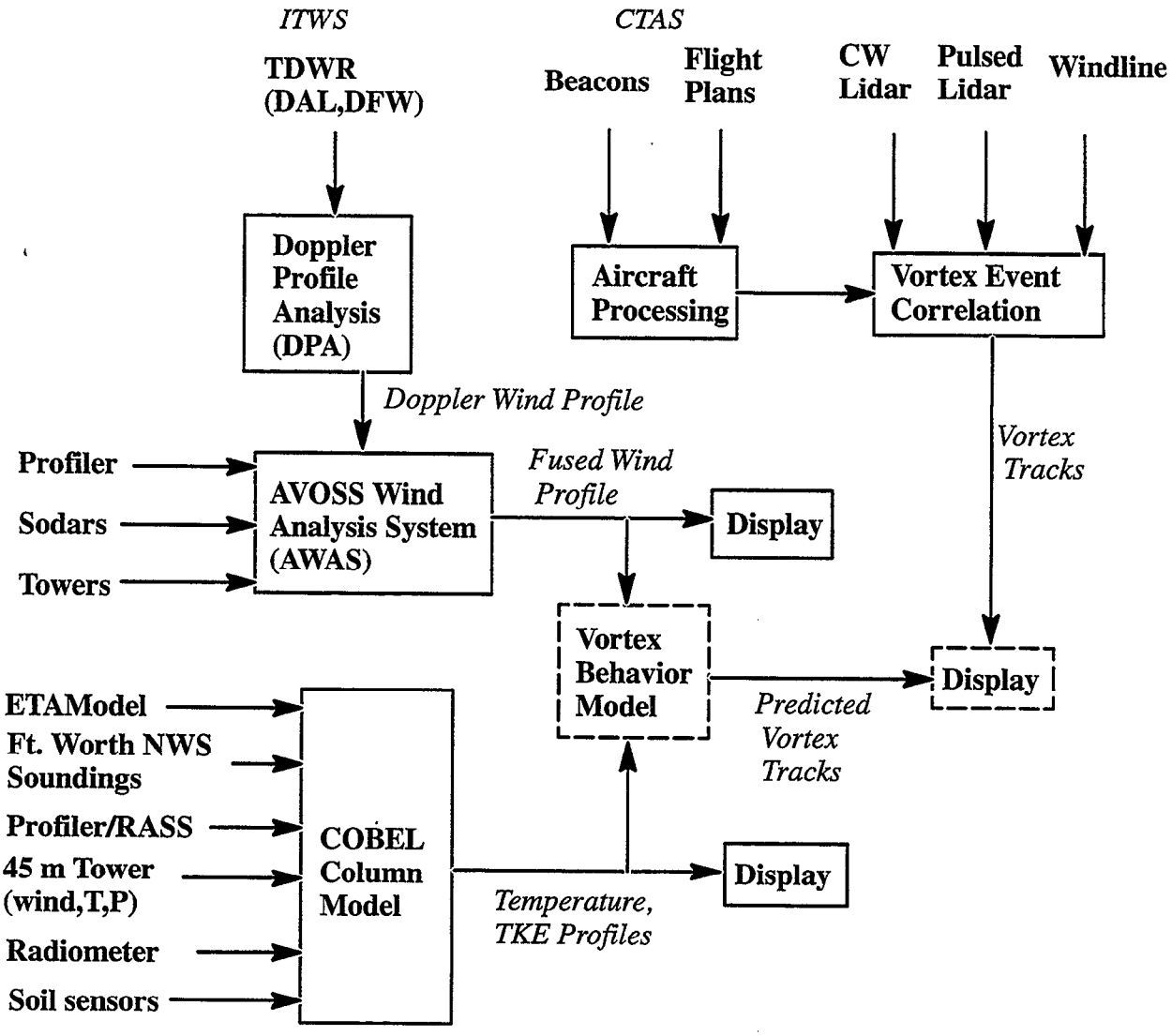

Figure 4. The functional organization and connectivity for the wake vortex processing algorithms. NASA–generated software modules are indicated by the dashed lines.

Table 1.
Functional Descriptions of Each of the Processing Modules in Figure 4

Module	Description
Doppler Profile Analysis (DPA)	Estimates a wind profile for the region around the airport using Doppler radar data and an optimal least–squares technique. This process is summarized in section 4.3 of this report.
AVOSS Wind Analysis System (AWAS)	Estimates a profile of the mean horizontal wind and the wind variability at the airport using the Optimal Estimation style of data fusion of most of the wind sensors available in DFW. This process is summarized in section 4.3 of this report.
Aircraft Processing	Associates aircraft beacon reports with the aircraft type in the corresponding flight plan. Estimates aircraft airspeed, groundspeed, descent rate, and track from beacon reports. Estimates time of passage of the aircraft through various windows along the final approach corridor. This process is summarized in section 5 of this report.
Vortex Event Correlation	Tags vortex tracks with the type of aircraft that generated the vortices. Adjusts the time of passage from the sensor tracks to correspond to the estimated time of passage from the beacon reports. This module is not described further in this report.
COBEL Column Model	A weather model that seeks to provide a physically consistent profile of the atmospheric conditions over the airport (Tardif et al., 1996). Can be run in diagnostic or forecast mode. Used in DFW to provide real–time diagnosed temperature and turbulence profiles. This module is not described further in this report, and data from this module is not included in the distribution.
Vortex Behavior Model	NASA Model which determines the safe aircraft arrival separations by predicting the range of vortex behaviors in the current atmospheric conditions. This module is not described further in this report.

3. VORTEX DATA COLLECTION AND PROCESSING

3.1. Continuous–Wave (CW) Lidar Design

The Coherent CW lidar operates by combining the atmospheric return with a reference on an optical detector. The interference between these signals creates a beat signal with a frequency related to the Doppler shift of the backscattered laser from motion of the atmospheric particles. At 10.6 μm the scatterers are primarily aerosols. The lidar design (Figure 5) is similar to those used in previous works (Huffaker, et al., 1970; Burnham, 1977; Koepp, 1991; Constant, et al., 1994), but with some significant improvements. First, the reference laser is offset in frequency from the primary laser by 10 MHz in order to resolve positive and negative Doppler shifts. The design also features a fully digital signal processing (DSP) system which offers greater flexibility than the analog techniques previously used.

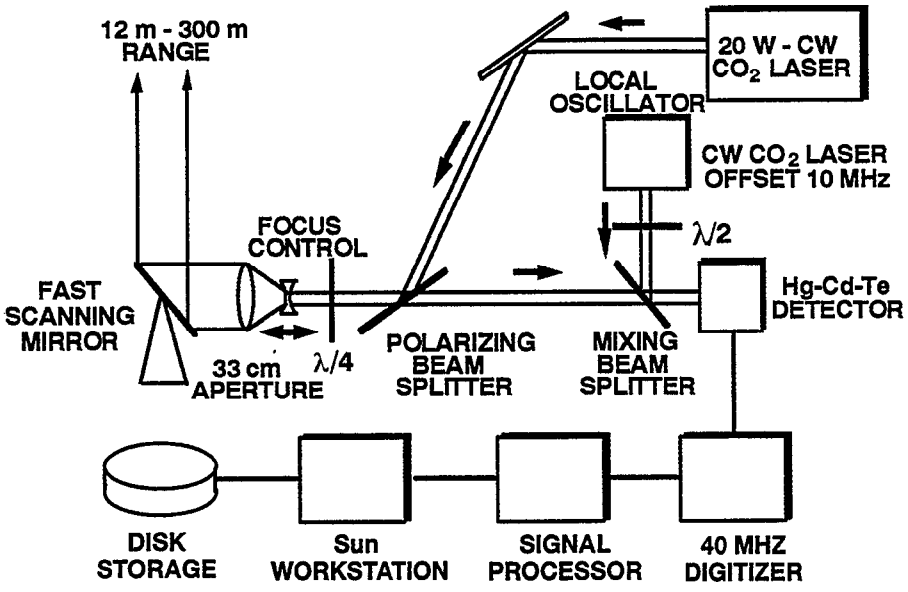

Figure 5. Wake vortex detection CW lidar design.

A CW lidar collects data by adjusting the focus range of the transmitted laser and scanning the beam across a region of interest. The lidar utilizes a 20 W CO_2 laser and a 33 cm aperture which provides an effective range resolution (related to the depth of focus) of ~6 m at 100 m range. The range resolution increases as the square of the distance, which restricts the practical maximum measurement range to roughly 300 m. This range limitation was the primary reason that the wake vortex observations were almost entirely of landing aircraft. The lidar collects data while sweeping a range of angles in a vertical plane while at a constant focus range. The maximum sweep rate is in excess of 180°/s, but typical scan rates are between 30°/s and 60°/s.

The backscattered laser radiation is collected by the lidar transmit/receive aperture and directed onto a HgCdTe detector along with the reference laser beam where they create a beat signal at their difference frequency. This beat signal is measured by the detector and is then amplified, filtered and digitized with a 10–bit analog–to–digital converter at a 40–MHz rate. Since the Doppler shift (Δv)

of the backscattered radiation is related to the line–of–sight velocity of the scatterers by $\Delta f = 2\Delta v/\lambda$, the 20 MHz Nyquist frequency of the digitizer corresponds to a 106 m/s velocity bandwidth for the λ=10.6 μm wavelength of the lidar. The 10 MHz offset of the reference laser shifts this to an effective –53 m/s to +53 m/s velocity dynamic range. During the 1997 DFW field measurements, the system was arranged to continuously digitize 256 x 18 points, requiring 115 μs at the 40 MHz rate. These data were then stored temporarily in a buffer, while a Sharp LH9124 digital–signal–processor (DSP) calculated 18 individual power spectra, each containing 128 points and corresponding to a velocity resolution of 0.8 m/s. These power spectra were then averaged together and the single averaged spectra were sent to one of the Sun workstations. The Sun workstations collected these power spectra in this mode at an average rate of 300 Hz.

For further information on the Lincoln CW lidar, readers should refer to previously published works (Campbell, et al., 1997; Heinrichs, et al., 1996; Heinrichs, et al., 1995).

3.2. Scanning Strategies

The lidar system typically is oriented so that the scan plane of the lidar is perpendicular to the extended runway centerline. For vortex generation altitudes that are out–of–ground–effect, the lidar is usually sited as close to directly underneath the aircraft as is possible. For vortices generated closer to the ground, the lidar is placed off to the side of the flight path. The lidar also has the capability to slant the fast scanning mirror down in the direction of the flight path, but this is generally used only when the lidar is in wind profile generation mode or when there is light rain (in light rain, a rain cover can be placed over the scan mirror to protect its surface).

The lidar scans in arc–scan mode, where the focus range is held constant and the beam is scanned through a series of angles. The rate of scanning is adjustable and usually is made to increase linearly with the focus range so that an approximately constant cross–range sampling resolution is maintained. After one of these arc–scans is completed, the lidar processes the information and chooses a new focus range for the next scan. Typically less than 0.5 s is required to change the focus range, perform the necessary processing, and start the next scan.

There are three scanning modes of the lidar used at DFW. They are summarized in Table 2, along with the parameters used in the 1997 DFW deployment. When vortices are not present, the lidar is sent into wind scanning mode. In this mode the lidar estimates a vertical profile of the horizontal winds. For wind profiling, a high velocity resolution and a frequent profile update rate are preferred. The lidar is put into a fast scanning mode to accomplish frequent profile updates. Just prior to an aircraft passage, the lidar is placed into vortex acquisition mode by the lidar operator. In this mode, the lidar is sent through a preprogrammed periodic scanning sequence that scans around the expected area of vortex generation. An automatic vortex detection algorithm is always activated (even in wind mode) to try to determine whether a vortex signature is present in that scan. If a vortex is detected when the lidar is in vortex acquisition mode, the lidar automatically switches to vortex tracking mode and begins to follow the vortices. The lidar can be instructed to follow either vortex or both. An example that shows the lidar adjusting its focus range and scanning angles to track a vortex is shown in Figure 6.

Table 2.
Lidar Scanning Mode Characteristics

	Wind	Vortex Acquisition	Vortex Tracking
Velocity resolution	0.1 m/s	0.4 m/s	0.4 m/s
FFT Rate	~75 Hz	~300 Hz	~300 Hz
Scan Speed @ 100 m	180 °/s	60–90 °/s	30–60 °/s
Next Scan	pre–programmed	pre–programmed	based on vortex location
Inter–Scan Processing	search for vortices and compute wind profile if none found.	search for vortices; switch to vortex tracking mode in range or angle if vortex range or angle could be computed.	detect and follow vortices

3.3. Vortex Tracking Algorithm

After an aircraft passes through the scan plane of the lidar, an automatic vortex detection and tracking algorithm is used to adjust the focus range of the lidar and the range of angles over which it scans. The result is a much more efficient scanning pattern, which allows for more frequent updates of vortex position and circulation and generally keeps the focus of the lidar system closer to the vortex core.

A real–time detection and tracking algorithm was first used in Memphis in 1994 (Dasey and Heinrichs, 1995), and a slightly modified version used in the 1995 Memphis deployment was described in the Memphis Data Guide (Campbell, et al., 1997). The detection and tracking algorithm was upgraded for the DFW demonstration as described in the coming sections. The basic scheme of the real–time algorithm is to estimate the location of the vortex core in angle, perform an intelligent interpolation amongst a sequence of lidar scans to determine the vortex range from the lidar, and then perform a scan selection procedure to determine the next lidar focus range and scan angle based on the lidar position estimate.

3.3.1. Vortex Angle Estimation

Previous incarnations of the vortex detection algorithm determined the vortex core angle by convolving an idealized vortex velocity profile with the maximum tangential velocity profile of each

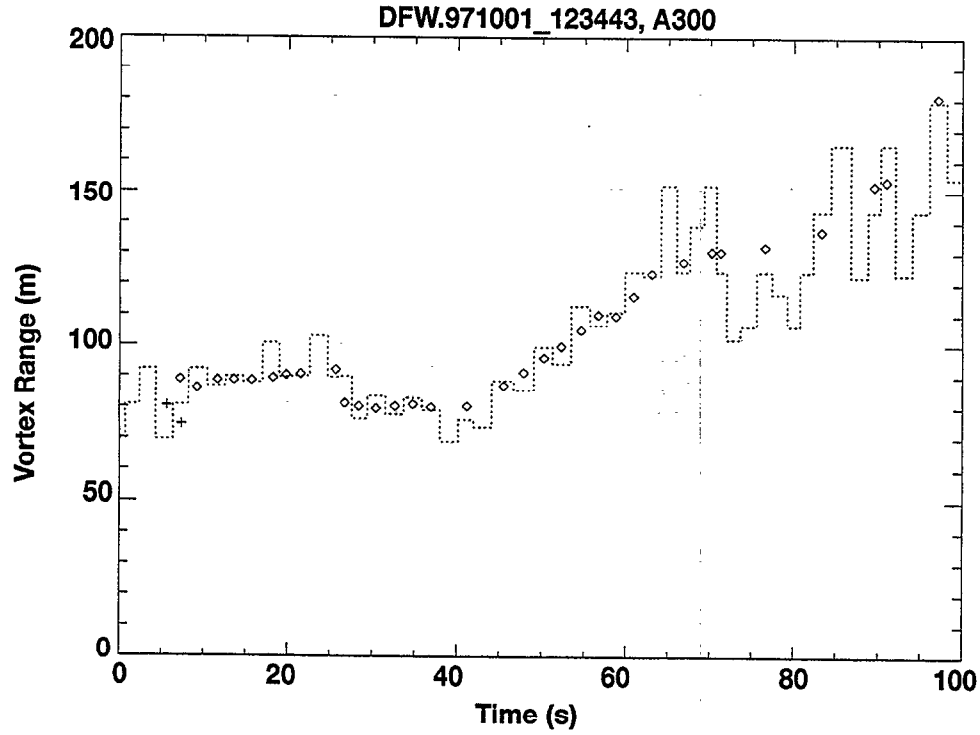

(a)

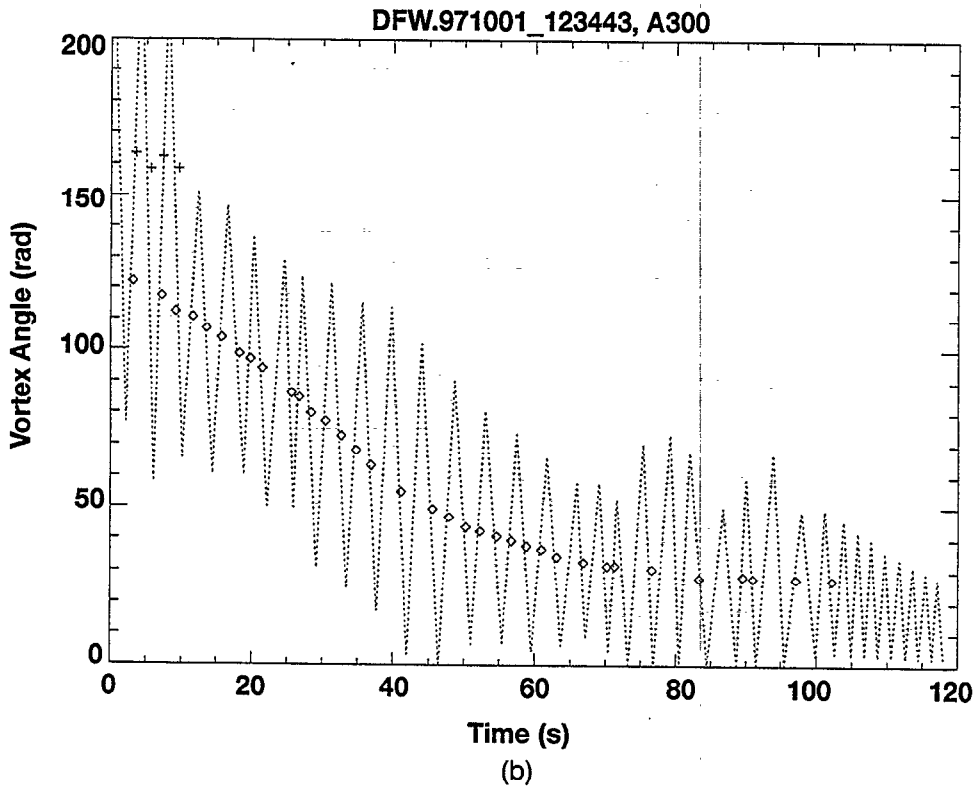

(b)

Figure 6. Examples of the lidar tracking a wake in (a) scan angle and in (b) range. The dotted lines show the range of scan angles and focus ranges selected by the real–time tracking algorithm. The detected angle and range of the port (diamonds) and starboard (plus signs) vortices are also shown.

scan that was measured by the lidar.[1] Convolution values whose amplitude was above a user–defined threshold were declared to be vortices, with the location of the core identified as the angle with the peak convolution. The sign of the convolution determined the sign of vorticity. This method is computationally efficient and fairly effective with strong, well–defined vortices, but it suffers from some deficiencies. Chief among these shortcomings is the sensitivity that the algorithm has to "noise." Since only a single velocity estimate is being used per velocity spectrum collected, if that velocity estimate is in error, odds of a false vortex detection are high.

The angle detection technique was modified for use at DFW, with the result that more of the spectral content is used in determining whether a vortex is present in any scan. Figure 7 shows the sequence of steps that are used for determining the vortex angle. Prior to the aircraft passing overhead, the mean (μ) and standard deviation (σ) of the spectral power as a function of velocity are determined. The first step in angle detection is to convert the velocity spectra to binary by comparing the spectral power at each velocity bin with the power that is n standard deviations above the spectral mean prior to aircraft passage. That is

$$\begin{aligned} T_k &= 0 \text{ if } S_k < N_k \\ &= 1 \text{ if } S_k \geq N_k \end{aligned} \tag{1}$$

where k is the velocity bin, T is the binary thresholding image shown in Figure 7(b), S is the original spectrum shown in Figure 7(a), and N is the predeterming noise floor, determined as

$$N_k = \mu_k + n^*\sigma_k \tag{2}$$

The parameter n can vary from day to day, but is generally chosen to be in the range from 4 to 10. After the spectra are binary thresholded, scoring functions are formed that weight the relative likelihood of the presence of the port and starboard vortices. These scoring functions are computed as the convolution of a two–dimensional function with the binary thresholded image T. Figure 8 shows a pictorial of the convolution operator that is applied to T to compute the port and starboard scoring functions, where this operator is being applied to a velocity vs. cross–range distance image T, an example of which is shown in Figure 7(b). The port vortex looks in quadrants A and D based on the expectation of vortex velocities greater than the line–of–sight ambient wind velocity bin (ω) at scan angles greater than the vortex core angle and velocities less than ω for scan angles less than the vortex core angle. The size of the window is controlled by the parameters δ and ψ, and were typically set at $\delta = 10$ m and $\psi = 30$ m/s for the DFW deployment. In addition to the higher resistance to noisy maximum velocity estimates that this provides in relation to previous algorithms, this technique has the advantage that vortices at the same angle with respect to the lidar can both be detected even though contributions from more than one vortex may be in any one spectrum. The scoring functions are normalized by the number of velocity bins that are searched in each quadrant to provide more constancy in values over various velocity resolutions and scanning speeds.

A vortex is declared found if the largest value of the port or starboard scoring function exceeds a threshold. This threshold can be actively adjusted through a graphical user interface by the lidar operator. The vortex core angle is the scan angle with the highest value of the scoring function.

1. An explanation of the method for determining the maximum tangential velocities, which are also used in the circulation estimation technique, is given elsewhere (Heinrichs and Dasey, 1997).

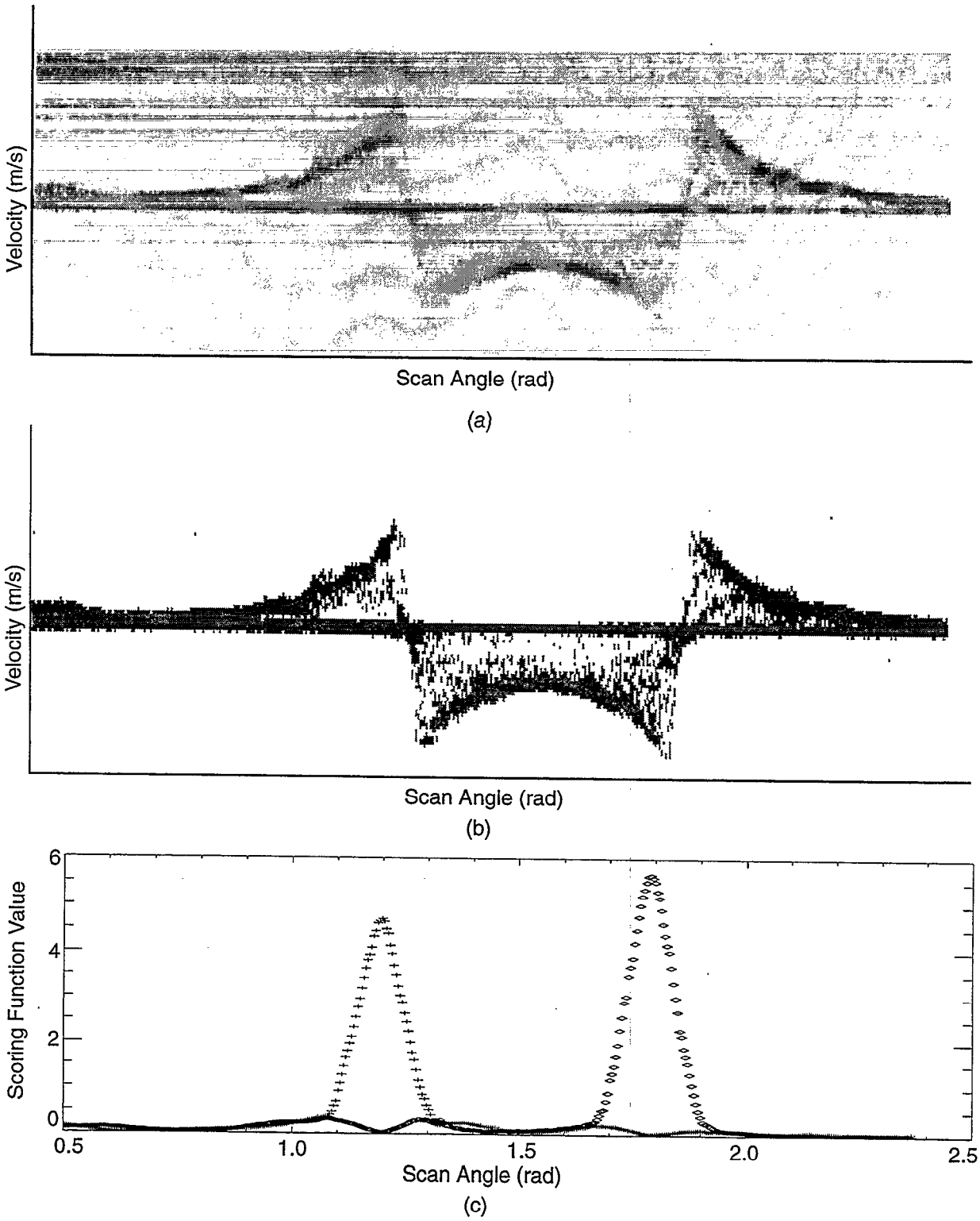

Figure 7. The sequence of steps in determining the vortex angle. The original spectra in (a) are amplitude thresholded to form the image in (b). Then a two–dimensional convolution operator is applied to (b) to determine the scoring functions in (c). The peaks in (c) are used to determine the existence of a vortex and their core scan angle.

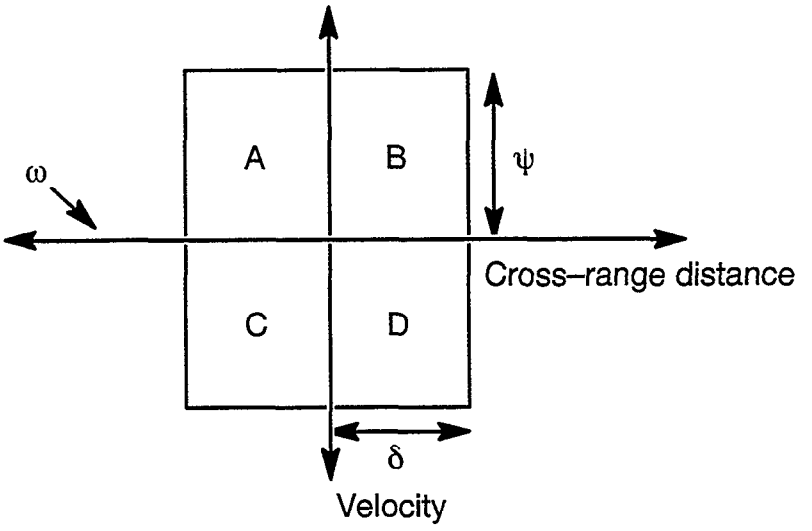

Figure 8. Pictorial of the two–dimensional window that is convolved with the binary thresholded image to produce the scoring functions. The center of the window is at the cross–range position of the current spectrum. To find a port vortex, all of the pixels in quadrants A and D are 1.0, while the pixels in B and C are 0.0; the starboard vortex scoring function uses A and D as 0.0, and B and C as 1.0.

Figure 7(c) shows examples of the port (plus signs) and starboard (diamond) scoring functions for the scan shown in parts (a) and (b).

3.3.2. Vortex Range Estimation

The technique for determining the vortex ranges is identical to the one used in the Memphis post-processing (Campbell, et al., 1997; Salamitou and Hansmann, 1995). The algorithm was ported to the real–time lidar system between the Memphis deployment in August of 1995 and the first JFK measurements in November of 1996.

3.3.3. Scan Selection

Once the vortex position has been determined, the software decides where the next scan should go by choosing a range of mirror scan angles and a focus range. The chosen angles and ranges are determined according to the previously documented procedure (Campbell, et al., 1997).

3.4. Vortex Data Processing

The lidar spectral data are reprocessed afterward in order to ensure that the highest quality data set is provided to researchers.

3.4.1. Vortex Position Estimation

Identical vortex angle and range estimation procedures are used as described in Section 3.3., but an additional step is included. The vortex angle detections from the algorithm described in Section 3.3.1. are manually checked and corrected on a scan–by–scan basis by a trained analyst. The range estimation procedure is then run as is done in real time.

3.4.2. Vortex Circulation Estimation

This section presents details of the procedure used for estimating the circulations from data collected during the DFW campaign. The inputs to the calculations include the raw spectral files and the vortex position estimates, which include vortex angle and range estimates for each scan. The vortex position estimates are made only from scans for which there is a clear vortex signal, which is determined by a manual editing procedure. The algorithm output includes circulation values calculated over a set of radius regions, each 1 m wide, centered at 1 m intervals out to 25 m on each side of the vortex core. The circulation–estimation procedure has been updated since the processing of the Memphis and JFK data, although the basic calculation algorithm has remained unchanged. The circulation–estimation procedure is as follows:

1. The first 100 spectra in the raw spectral file are used to calculate the average value and standard deviation of the signal in each velocity bin. These typically represent the spectral output in the absence of a vortex signal.
2. The spectra are sorted according to lidar scans, where a lidar scan corresponds to a continuous motion of the scan mirror with the system set at a constant focus position. Subsequent processing is then performed on a scan–by–scan basis.
3. The vortex range and angle estimate for each scan is read from the vortex tracking file (generated previously with the tracking algorithm) and a crossrange is calculated relative to the vortex core given by the product of the vortex range and the relative angle from the core.
4. For each scan, the modified–maximum velocities are then calculated from the raw spectra at crossrange values within 25 m on either side of the vortex core. The modified–maximum velocities are basically the maximum velocities of each spectra, six standard deviations above the average, reduced by an amount determined from the spectral spreading due to the time–series windowing and the amplitude and proximity of the nearest spectral peak. These velocities are calculated twice for each spectra: once for the positive velocities and once for the negative velocities.
5. The modified maximum velocities versus crossrange for each scan are then assembled by taking the positive velocities on one side of the core and the negative velocities on the other side of the core. Which sides of the core contain the positive or negative modified maximum velocities is dependent on whether the port or starboard vortex is considered.
6. The modified maximum velocity versus crossrange for each scan is then fit to a Lamb vortex model, using a standard gradient–search technique nonlinear least–squares curve-fit routine. The fit parameters include the crossrange position of the core, the width of the core region, and the vortex velocity at the core radius. Only the crossrange position of the core from the fit is used. This parameter is used to adjust the crossrange so the center of the vortex is more accurately located at the zero crossrange position. This adjustment is typically less than 1 m. If the core position determined from the fit differs from the position in the vortex tracking file by more than 1.5 m in crossrange, then the vortex scan is not processed for circulation estimation.

7. The circulation estimate is then calculated at 1 m crossrange intervals extending from –20 m to +20 m, with each interval 1 m in width. There are typically 1 to 3 velocity points per crossrange interval, depending on vortex range.

There are two main differences between this procedure and the one used to process Memphis data. The first is that the angle position determination of the vortex is no longer performed as part of the circulation estimation routine. Instead, the angle position from the vortex tracking file is used and modified only slightly by the results of fits of the velocity profile to a Lamb model.

The second difference involves the introduction of an automatic quality control mechanism for circulation estimation. The Memphis data was manually edited both for vortex angular position determination and quality of circulation estimation. The DFW data are manually edited only for angular position. The quality control for the circulation estimation is performed by checking that the vortex position fit parameter from the Lamb fits does not differ from the previously determined, angular position by more than a minimal amount. This criterion has been demonstrated empirically to be a good qualifier for high–confidence vortex circulation estimates from each vortex scan. This is demonstrated by Figure 9, which compares the results of vortex circulation estimation with and without the core position shift selection criterion. The circulation estimates which did not satisfy the criterion were clearly poor estimates in this case.

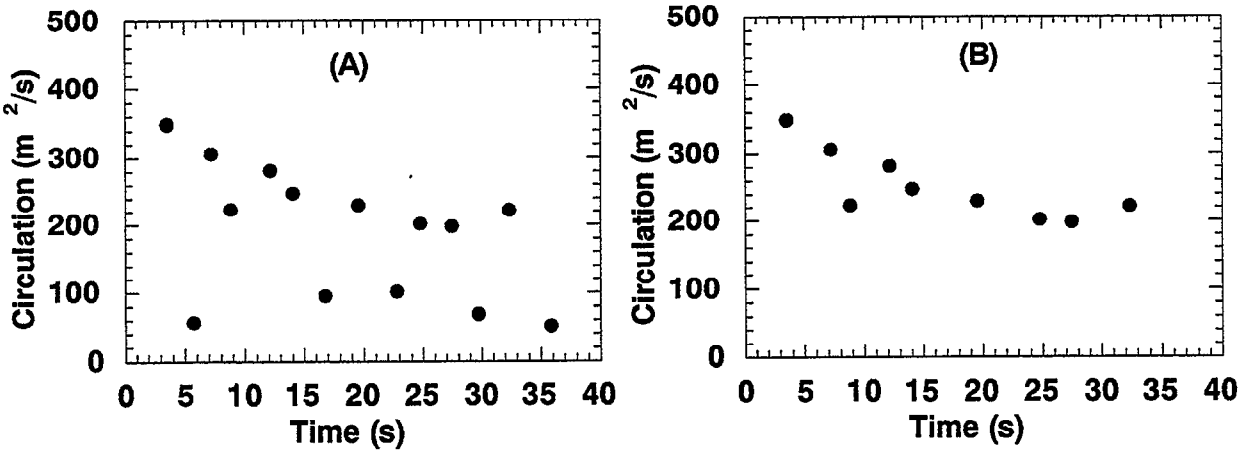

Figure 9. Estimated circulation versus time measured from an MD80 aircraft without the circulation point–selection criterion (A) and with the circulation point–selection criterion (B).

3.5. Alignment and Calibration Procedures

Primary Optical Bench Alignment

The primary optical bench alignment is performed only after major relocations of the lidar or after the system has been dismantled for upgrade. This alignment was performed upon arrival at DFW. This alignment procedure involves the correct positioning of the off–axis parabolic primary mirror and the variable focus translation stage. The basic procedure is to use a Twyman–Green interferometer to locate the optical axis of the parabolic mirror and position the variable focus stage parallel to this axis with the use of a tilt–sensitive interferometer. For this process, 632 nm radiation from HeNe lasers are used, and then the final alignment is transferred over to the 10.6 micron CO2 beam.

As part of this alignment process, the focal range calibration and lidar response function calibration are performed. The distance from the parabolic mirror at which the transmitted lidar beam comes to a focus is controlled by moving the focusing optics, which are mounted on a translation stage. The first step in the focal range calibration is to generate predictions of the focal distance from the parabolic mirror versus focusing lens position using a ray–tracing computer code. These predictions were then fit to an equation of the form:

$$\text{focus} = A/(B - x) + C, \tag{3}$$

where A, B, and C are fit parameters and x is the relative position of the focusing lens. The actual focal range is then measured by moving the focus lens assembly to various positions and then physically measuring the location of the laser focus from the truck and adding the extra distance to the parabola. These data were then used to determine the offset parameter, B, in the above equation, keeping the theoretical fit values for A and C.

Daily Optical Alignment

The daily adjustment of the lidar alignment included "tweaking" the optical components and verifying the position of the focusing optics and scan mirror. Tweaking the optical component involves verifying that the CO_2 beam is going through the optical axis of the variable focus system and that it is centered on the parabolic mirror, as well as checking that the backscattered beam and the local oscillator beams each are centered on the detector. The final optical adjustment tweaks the backscattered beam on the detector to optimize the signal from the ambient wind.

The daily focus lens and scan mirror calibrations are performed automatically by having the computer system do a fine position search for fixed hardware markers in both systems. These markers define very precise locations for the scan mirror angle and translation stage position and are accurate to within 0.04 degrees and 10 microns, respectively. Early testing demonstrated that the laser focal location was reasonably constant with respect to focusing optics position, so the external focus location is typically not checked on a daily basis. The marker position on the scan mirror is set to the vertical position relative to the roof of the truck, with an accuracy of about ± 1 degree. This would represent a systematic angle offset that would be common to all the data over a given push (after which the scan mirror is removed from its housing for shipping). The main source of error in the scan angle, however, is related to the accuracy in leveling the lidar truck after each change in location around the airport. This leveling is performed by centering level indicators near the rear corners of the truck, and the error associated with this process is estimated to be about ± 3 degrees. This error would be common to all data collected during the time that the lidar truck was positioned in one location and would vary once the lidar truck was relocated.

4. METEOROLOGICAL DATA COLLECTION AND PROCESSING

4.1. Site Layouts

The meteorological sensor suite was situated at two different sites at the Dallas Fort Worth International Airport.

4.1.1. North Site

The meteorological site on the north side of the DFW airport was located at 32.9169 north and 97.0378 west. The site is located 2500 feet west of the centerline of runway 35L, and 3900 feet east of the centerline of runway 36R. This places the north site slightly east of the center of the airport and slightly south of the runway 17R threshold. The secondary access road (North Service Road) is located 200 feet west of the site, with a gravel road leading from the service road to the meteorological site. An American Airlines cargo building is approximately 1000 feet to the south of the site.

Figure 10 shows the location of the various sensor systems and their orientation to one another at the north site. In the middle of the site is a 8–foot by 16–foot building (commonly referred to as the "shed"). The profiler/RASS is located 75 feet south of the shed, and the Sodar is located 120 feet north. The 10–meter tower is located at the south end of the site, approximately 240 feet south and east of the computer shed and 800 feet north of the American Airlines building. This orientation was chosen due to limitations in the distance from the computer equipment to the profiler and the Sodar.

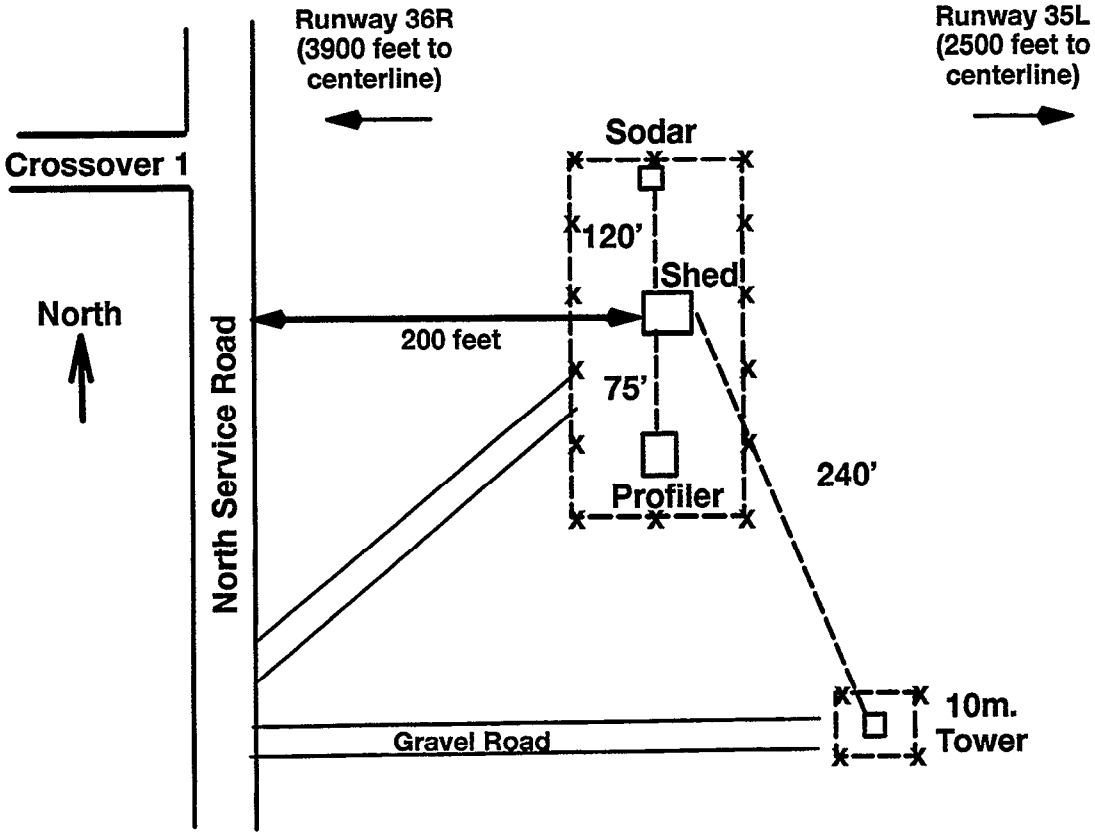

Figure 10. Dallas Fort Worth International Airport north meteorological site.

The shed houses all of the computer equipment necessary to run the profiler/RASS, Sodar, tower hardware, and communications equipment. The shed also was used to house the radiosonde computer equipment; all balloon launches on DFW airport occurred within a few meters of the building.

4.1.2. South Site

The meteorological site on the south side of the DFW airport was located at 32.8833 north and 97.0425 west. The site is located 2500 feet east of the centerline of runway 36R and 3900 feet west of the centerline of runway 35L. This places the south site slightly west of the center of the airport and slightly north of the runway 36R threshold. The secondary access road (South Service Road) is located 200 feet east of the site, with a gravel road leading from the service road to the meteorological site. A taxiway is located to the north of the site, approximately 400 feet, while a large, open grassy field is located to the south and west of the site. Some interference may be observable at the site during a northerly wind due to the elevated surface that the taxiway is built upon.

Figure 11 shows the location of the various sensor systems and their orientation to one another at the south site. On the north end of the site is the computer shed, similiar to the one at the north site. The Sodar is located 120 feet west of the shed. The 45–meter tower is located 200 feet due south of the shed. A 10–meter tower is located at the south end of the site, approximately 120 feet west

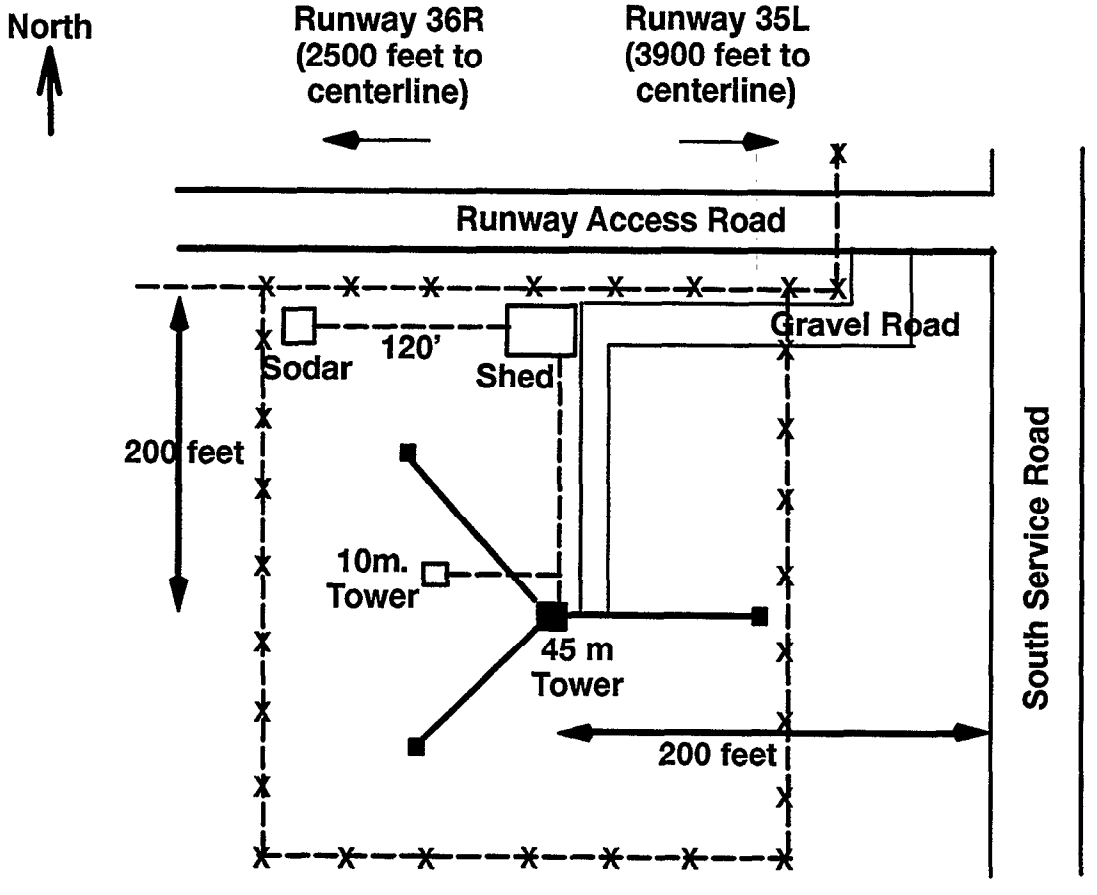

Figure 11. Dallas Fort Worth International Airport south meteorological site.

of the 45–meter tower. This orientation was chosen due to limitations in the distance from the computer equipment to the Sodar. The shed houses all of the computer equipment necessary to run the Sodar, tower hardware, and communications equipment.

4.2. Meteorological Sensors

4.2.1. Instrumented Towers

The meteorological towers are equipped with three different types of sensor packages. The first package, known as a SAVPAK, measures the standard atmospheric variables at a 1 Hz rate. The second, a FLUXPAK, uses a 10 Hz sonic anemometer to measure the atmospheric fluxes. The final tower–mounted package is the barometer. Figure 12 shows the locations of these packages on the 45–meter south site tower, Figure 13 shows the locations of these packages on the 10 meter south site tower, and Figure 14 shows the locations of these packages on the 10 meter north site tower.

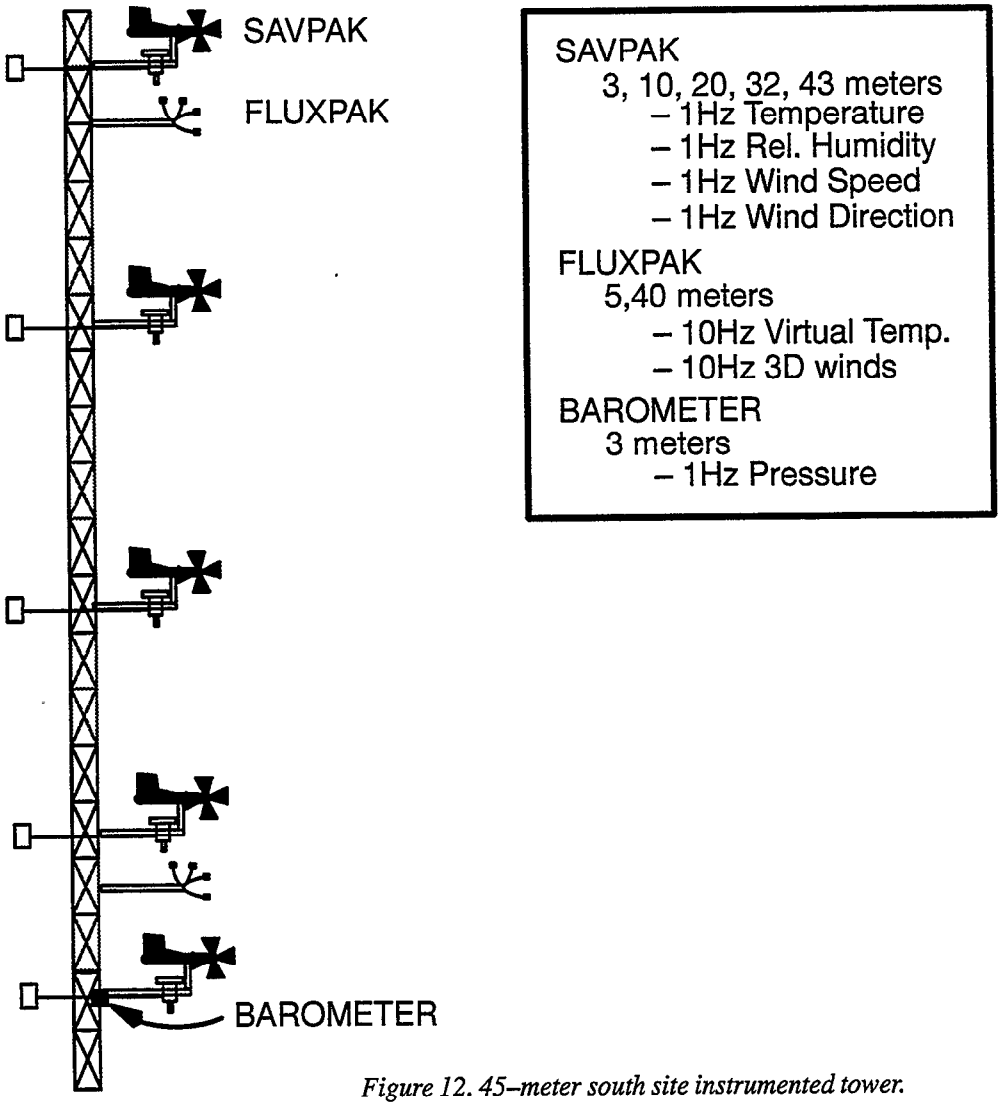

Figure 12. 45–meter south site instrumented tower.

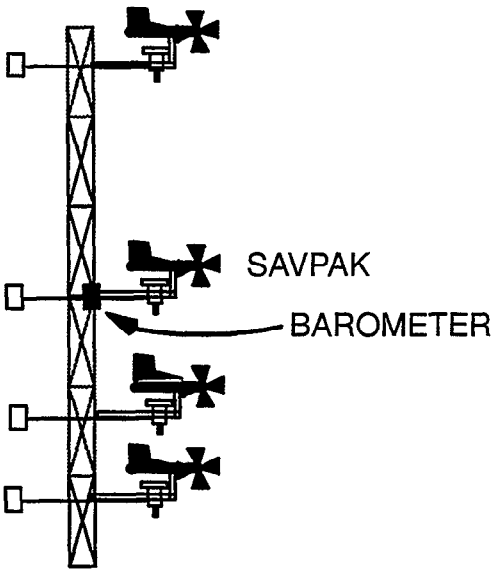

SAVPAK
1,2,5, 10 meters
– 1Hz Temperature
– 1Hz Rel. Humidity
– 1Hz Wind Speed
– 1Hz Wind Direction

BAROMETER
5 meters
– 1Hz Pressure

RADIOMETER
2 meters
– 1 Hz Net Radiation
– 1 Hz Radiation IN
– 1 Hz Radiation OUT

SOILPAK
2, 10, 100 cm.
– 1Hz Temperature
– 1Hz Moisture
– 0.1 mm Rain (sfc.)

Figure 13. 10–meter south site instrumented tower.

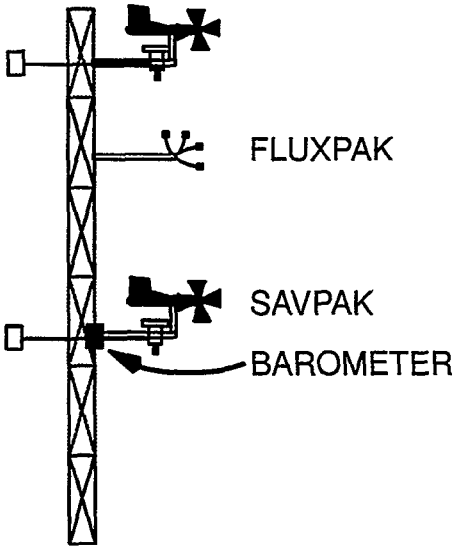

SAVPAK
5,10 meters
– 1Hz Temperature
– 1Hz Rel. Humidity
– 1Hz Wind Speed
– 1Hz Wind Direction

BAROMETER
5 meters
– 1Hz Pressure

FLUXPAK
8 meters
– 10Hz Virtual Temp.
– 10Hz 3D winds

RADIOMETER
2 meters
– 1 Hz Net Radiation
– 1 Hz Radiation IN
– 1 Hz Radiation OUT

SOILPAK
2, 10, 20 cm.
– 1Hz Temperature
– 1Hz Moisture
– 0.1 mm Rain (sfc.)

Figure 14. 10–meter north site instrumented tower.

The SAVPAK measures four standard atmospheric variables: temperature, relative humidity (RH), wind speed and direction. This is done using two sensors manufactured by R.M. Young of Traverse City, Michigan. The first is the Temperature/Relative Humidity sensor, model 41372C, with the Gill Aspirated Radiation Shield, model 43410. The temperature measurement is in degrees Celsius, and the humidity output is in percent. The second instrument is the Wind Monitor–AQ, model 05305. The wind speed is measured in meters per second, with the wind direction given from 0–360 degrees.

The temperature sensor uses a 1000–ohm platinum resistance vs. temperature device (RTD) manufactured by R.M. Young. It has a measurement range of –50 to 50°C, with an accuracy of 0.3°C. Sensor output is an analog signal between 0 and 1 volts. Conversion of the analog output is done within the processing software. Calibration of the R.M. Young platinum RTD was performed by the manufacturer using the NIST standards. The humidity is measured with a Vaisala Intercap element, with a measurement range of 0–100 percent RH. It has an accuracy of two percent from 0 to 90 percent RH, and three percent from 90 to 100 percent RH. The sensor has an operating range of –10 to 60°C and a stability of ± 2 percent in two years. It produces an analog signal between 0–1 volts that is converted within the processing software. Calibration also can be performed on this instrument in a controlled environment.

The Gill Aspirated Temperature Shield consists of a horizontally–oriented hollow tube and a 24VAC blower mounted on one end, with the sensor on the opposite end. The blower constantly pulls the ambient air across the sensor and down the hollow tube to the blower. The shield employs a downward facing intake tube surrounded by a canopy that minimizes the direct and indirect radiation. The sensor mounts vertically in the center of the intake tube.

The Wind Monitor–AQ measures wind speed using a 20 cm diameter four–blade helicoid propeller carbon finger thermoplastic. It has a range of 0.4 to 40 m/s, with a gust survival of 45 m/s. The sensor output is an AC sine wave signal produced by a rotating magnet on the propeller shaft. A Wind Sensor Interface, also supplied by R.M. Young, converts the signal into an analog output of 0–1 volts. Wind speed accuracy is reported to be within two percent. The analog signal is converted to meters per second in the processing software.

Wind direction is measured using a balanced vane made of Styrofoam, with a turning radius of 48.3 cm. This lightweight design allows for a rapid response to wind direction changes. The sensor has a 360° mechanical range, with a 5° electrical opening at 355°. The sensor uses a precision conductive plastic potentiometer, 10K ohm resistance, to generate the analog signal of 0–1 volts. Wind direction accuracy is reported to be within one degree. The Wind Sensor Interface, mentioned previously, converts the 12VDC input power to an excitation input.

Each Wind Monitor–AQ is mounted on a one–inch diameter, vertically–oriented pipe at the specified tower heights. The pipe is mounted 36 inches off the tower by using another one–inch–diameter pipe. Each mounting structure is on the southwest side of the tower. Figure 15 shows a top view of the south site wind towers and the orientation of the wind sensors. Disruption of the ambient wind is possible when the wind is blowing through the tower structure, between 20 and 70 degrees. At the north site, sensor mounts were orientated to the northeast, so disruption may occur with winds blowing between 200 and 250 degrees.

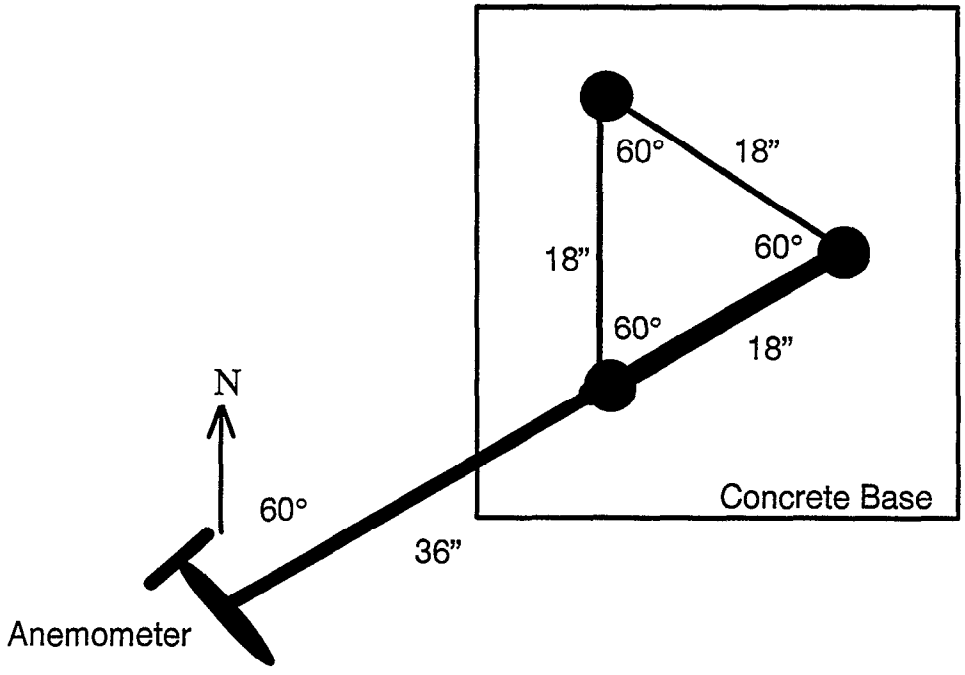

Figure 15. Orientation of Wind Monitor to tower structure.

Alignment is performed on each sensor using the R.M. Young Vane Angle Fixture—Tower Mount, Model 18212. First, an alignment ring is secured to the pipe, then the Vane Angle Fixture, and finally the sensor. The vane angle fixture consists of a large compass that will hold the sensor aligned in one fixed direction. Using a known point on the horizon, the sensor can be visually aligned. Finally, a comparison of the known angle and the measured angle is performed. Realignment is performed if the difference is not within threshold.

The FLUXPAK uses a sonic anemometer to measure the three–axis component of the winds and the virtual temperature at a 10 Hz rate. The sonic anemometer used was manufactured by Applied Technologies, Inc. of Boulder, CO. The sensor transmits and receives a sonic signal along a fixed orthogonal direction, and from this determines the component of the wind. It also determines the sonic temperature of the measured winds from the vertical sonic measurements. The sonic has a measurement range of ± 15 m/s for the three–axis winds and a range of –20 to 50 °C for the temperature. The wind accuracy is ± 0.05m/s and ± 0.05 °C for the sonic temperature. The absolute temperature accuracy is ± 2 °C. Data output is a serial RS–232C compatible format that is easily interpreted in the processing software.

At the base of each tower is a barometer. The barometer is a Model 61201 Barometric Pressure Sensor from R.M. Young Inc. It has a measurement range of 800–100 millibars, with an accuracy of 0.5 millibars. The unit is contained within a waterproof case and connected to the Model 61002 Gill Pressure Port. The pressure port minimizes dynamic pressure errors caused by wind flow over the barometer inlet. The unit produces a 0–5VDC signal that is converted to millibars within the Campbell Scientific datalogger.

4.2.2. Profiler/RASS

The profiler is a remote sensing Doppler radar capable of determining the wind speed and direction for several different altitudes. The profiler is a 915 MHz system with a four–beam phased array antenna. The unit is manufactured by Radian Corporation of Boulder, CO. The RASS option on the profiler is capable of providing the virtual temperature and operates at 2000 Hz.

The profiler has a range of parameters that the user may specify for operations. The minimum measurement height parameter was set to 145 meters, and the maximum measurement height was set to 4,881 meters. The profiler was operated with a vertical resolution of 97 meters at a 700 ns pulse. The profiler has a wind speed accuracy of 1 m/s and a wind direction accuracy of 10 degrees. Time averaging of 25 minutes was performed every half hour, allowing a five–minute gap for RASS operations.

The RASS parameters also can be controlled by the operator. For the installation in Dallas, the parameters were set to a minimum height of 127 meters, with a vertical resolution of 105 meters. The maximum height allowed was 1,492 meters. The temperature accuracy of the RASS is reported to be 1 °C. The RASS was operated with a five–minute averaging time, performed at the end of each 25–minute wind sampling period.

4.2.3. Doppler Sodars

A sodar provides time–averaged horizontal wind vector and the vertical wind speed. It also provides a measure of the wind variability. The sodars are located 120 feet from the shed, and the data cables were placed inside a buried conduit for protection. The PC performing the time averaging was located inside the shed, and a serial line was provided from the PC to a Sun workstation.

The Remtech PA2 sodars were used to measure the winds from 50 meters to 600 meters at a frequency near 2200 Hz. The time–averaging was operated at five minutes, with a 20–meter vertical increment. The Remtech PA2 sodars appeared to have performed well, even within the high noise environment of the airport. The sodars are the only DFW data source that tag the data with the end of the averaging period. All other sensors use the start of the averaging period. There also appeared to be very little interference between the sodar and the RASS mentioned earlier.

4.2.4. Balloon–LORAN System

During the deployment, a LORAN CLASS balloon sounding system owned by the University of Massachusetts at Lowell, Meteorology Department, was used for measurements of temperature, pressure and winds. Balloons were launched daily, six times per day for two weeks of the deployment. The radiosondes were launched from the shed at the north meteorological site. Since this site was between the two primary active runways, launches needed to be closely coordinated with air traffic personnel.

The CLASS sounding system consists of a disposable Vaisala RS80 sonde which is attached to a 200–gram balloon, a receiver located in the shed, a LORAN–C NORTHSTAR 800 processor, a Vaisala PP–11 processor, and a 386PC. The sonde contains a LORAN receiver that receives a signal from the LORAN system. The LORAN signal, along with an encoded signal from the meteorological sensors, is transmitted back to the shed where another receiver takes the signals and splits them

into two components: one to the LORAN processor (position information) and one to the Vaisala processor (meteorological information). The Vaisala processor converts the input signal into temperature, humidity, and pressure and passes that along to the 386PC. The LORAN processor converts the signal it receives into latitude and longitude and sends it to the PC. The PC logs all the data onto disk for post processing. Typically, the PC will produce a data point every two seconds.

The final step is to postprocess all of the archived data into a consensus file. This step is performed on the PC after the balloon has exploded and the sonde begins to descend to earth. The two–second data from the temperature, pressure, and humidity data sources is averaged into 10–second intervals. The vertical resolution of these intervals depends upon the amount of helium loaded into the balloon. Typically, the data has a 50–meter resolution. Finally, the latitude and longitude information is used to determine the movement of the balloon, thus estimating the winds. These data points are averaged over a 60–second interval. The first reported wind measurement is at 300 meters altitude.

4.2.5. Terminal Doppler Weather Radar (TDWR)

The Terminal Doppler Weather Radar (TDWR) was developed by the FAA to provide wind shear protection at most major airports in the country. The TDWR is a C–band pencil–beam Doppler radar with a 1–degree beamwidth. The radar performs full volume scans approximately every five minutes, with different scan strategies depending upon the weather conditions. The first mode, known as monitor, is used in clear air. In this mode, the radar performs 16 plan position indicator (PPI) volume scans. Each PPI is at a different elevation angle, ranging from close to the surface (0.1 – 0.3 degrees) to high elevation angles (approximately 60 degrees). The second mode, known as hazardous, is used when reflectivities in the radar scan region exceed a predetermined threshold indicative of rainfall or high cloud water content. In the hazardous mode, the radar performs a sector scan of 105 degrees centered on the airport. Two volume scans from the surface to roughly 60 degrees are performed in each five–minute period, with three full 360 degrees PPIs for gust front detections.

In the Dallas/Fort Worth area, two TDWR radars provide coverage over the DFW airport. The first, located 21 kilometers to the northeast of the airport, is the primary TDWR providing wind shear protection for the DFW airport. The second, located 8 km to the east–northeast, provides wind shear protection for the Dallas Love Airport (DAL). However, because of its proximity to the DFW airport, it provides excellent wind measurements over the airport during clear air mode.

The TDWR data are used to estimate horizontal wind velocity profiles. The algorithm for generating these profiles, termed the "Doppler Profile Analysis" (DPA), was created as part of this wake vortex project and performs according to the following steps:

1. *Quality Checking:* Dealiased and clutter–edited TDWR radial velocity data, in polar coordinates, are quality checked against corresponding signal–to–noise and reflectivity data. Radar gates with a signal–to–noise less than 7.0 or a reflectivity greater than 41 dBZ are declared as invalid velocity values. This is used to suppress using velocity data in very clear air conditions or in conditions where the vertical velocity component could be significant. Only DFW radar tilts at 0.3, 1.0, 3.8, 6.1, 11.0, and 15.9 degree elevation angles, and DAL radar tilts at 0.1, 0.3, 1.0, 2.6, 5.3, 6.1, 7.9, 10.4, 11.0, 13.0, 15.3, and 15.9 degree elevation angles are used. The DFW radar appears to use fewer elevation angles because the angles used in hazardous mode are identical to those used in monitor mode, while the DAL uses different angles in different modes.

2. *Median Filtering:* The edited radial velocity data is median filtered using a 1 km–by–1 km window. The number of gates within the median window vary with range.

3. *Resampling:* At the end of each volume scan, polar radial velocity data from the multiple tilts comprising that volume are resampled into a 2 km–by–2 km–by–50 m Cartesian grid, assuming a 0.3 degree beamspread. Polar data within each Cartesian grid point is combined using a weighted average. The 50 m resampling is organized so that the 50 m altitude level uses data from 25 to 75 m.

4. *Clutter Filtering:* To further reduce the chances of clutter breakthrough, resampled grid points with absolute velocities below 1.25 m/s are declared invalid for use in further analysis. This threshold has since been made dependent on the mean wind speed, but during the deployment, when winds were seldom calm, this change is not thought to have much of an effect on the resultant profile.

5. *Gauss–Markov Theorem:* Horizontal wind mean and variances are estimated by application of the Gauss–Markov theorem to the Cartesian resampled velocity data at each height level. The Gauss–Markov Theorem is described in Section 4.3.2. The horizontal extent of the data used to generate the mean and variance estimates can vary by altitude level, and also depends on the percentage of valid points near the radar. At low altitudes, the estimates are based on data within 5 km of the radar when more than 10 percent of the points within that distance are valid to as much as 10 km if more than a 5 km search is needed to find 10 percent valid data. These distances increase to as much as 15 km and 30 km at higher altitudes. Data used by the Gauss–Markov Theorem is weighted by inverse distance from the radar

4.2.6. Miscellaneous Sensors

At the base of the tower several instruments were located to determine the soil characteristics as well as the solar radiation and rainfall. Since all of these instruments were connected to a Campbell Scientific CR 10 datalogger, logging, averaging, and formatting were performed there in a similar manner. These instruments are used mostly for meteorological model initial state characterization. All were mounted on an aluminum frame consisting of three cornerposts with cross pieces.

The rain gauge model TE525 was manufactured by Texas Electronics and uses a tipping–bucket mechanism of 0.01–inch increments. The accuracy is within 1.0 percent at two inches per hour or less. It can operate at temperatures from 0°C to 50°C. The instrument produces an electronic pulse each time the bucket tips. The Campbell CR10 counts the pulses in a one–minute period and then sends a format ASCII text line to the serial port.

The radiometer, located at the southern post of the mounting frame, is a THRDS7 model from Radiation Energy Balance Systems (REBS) of Boulder, CO. The THRDS7 contains two high–output, 30–junction thermopiles with nominal resistances of 2 ohms each. It generates a millivolt output proportional to the temperature gradient across them. One thermopile is mounted on the top, the other on the bottom. A temperature sensor is located within the core of the sensor. A radiometer ventilator is used to continuously blow air across the sensor. The ventilator consists of a 12 Vdc blower that is mounted on the bottom side of a hollow tube. Without the ventilator, dew can build up on the radiometer, preventing accurate measurements.

The total hemispherical radiation can be computed from the thermopile voltages and the inner air temperature of the core. The incoming radiation is computed by looking at the top hemisphere of the sensor, and the outgoing radiation is computed by looking at the bottom hemisphere. From the incoming and outgoing radiation, the net radiation can be calculated.

The soil temperature and moisture were determined by two sensors, manufactured by Campbell Scientific, Inc. The 107B temperature probe measures temperature over a range of –35 to +50°C. The 107B is a platinum resistance temperature probe with a nominal resistance of 100 ohms. It has an accuracy of 0.2°C. The instrument was buried at depths of 2, 10, 20, and 100 cm at the two sites. The soil moisture probe was the CS615 Water Content Reflectometer. The accuracy of this sensor is two percent when calibrated for a specific soil. The water content is derived from the effect of changing dielectric constant on electromagnetic waves propagating along a wave guide.

4.2.7. Campbell Scientific Dataloggers

All data from the towers, barometers, soil sensors, rain gauges, and radiometers is logged and processed by a Campbell Scientific CR10 datalogger. The datalogger contains the software and electronics provided by Campbell Scientific. A script programmed in the CR10 data language performs a series of functions that the user can instruct the datalogger to perform. At the tower site, the datalogger is instructed to read the input data sources. Then, the datalogger performs the equations necessary to convert the data from its analog input to a digital signal. Next, the datalogger averages the data over a one–minute period, except in the case of the rain gauge, where the datalogger counts the number of input pulses over a one–minute period. Finally, the output data are sent to a serial port for transmission to a display or data reader.

4.2.8. CW Lidar Crosswind Profiles

The Lincoln CW lidar was used to generate crosswind profiles during times when it was not actively tracking wakes. The headwind component was not estimated. Ambient wind velocity for each Doppler spectrum was analyzed for a prominent non–zero velocity wind peak. Velocity resolution during wind profile generation was increased over the resolution used in vortex tracking to 0.1 m/s. Zero velocity peaks from the automated algorithm were not used in the analysis due to possible contamination in that frequency bin from backscatter off of stationary system components. Line–of–sight wind estimates were binned into 10 m vertical bins according to the position of the lidar focus, and crosswind mean was determined for each vertical bin for each lidar scan by assuming zero vertical wind. The scan means (collected every 1–2 seconds) were assembled over a one–minute period to produce means and variances at each altitude level, generally up to a maximum of 400 m altitude.

4.2.9. Sensor Limitations

Limitations in the data exist depending upon the sensor, sensor alignment, wind direction, and weather. No data were removed from the database, based upon these known limitations. The acceptance or rejection of data based upon known limitations or analysis is left up to the user.

Data collected from the R.M. Young Wind Monitor–AQ (SAVPAK variables 15–18 wind speed, wind direction, u component, v_component) is suspect when the wind is blowing through the tower structure. During times of strong winds, this appears to be less of a problem.

Data from the ATI sonic anemometer (all FLUXPAK data) is questionable during times of heavy rainfall. If significant blockage of the beam occurs when raindrops are present, the data can become corrupt, or very few data points are used to compute the averages. Also, wind speeds in excess of 12 m/s are questionable from the ATI due to the sensor's limitation of 15 m/s maximum wind velocity for each of the wind components.

Data from the profiler/RASS and sodars are questionable during times of heavy rainfall. Whenever rainfall is present, analysis with other sensors should be performed to validate the quality of the data.

Balloon–LORAN system wind measurements were typically widely scattered. Even considering the short averaging times of these wind reports, the correlation with other sensors was generally weak and the balloon–LORAN system wind measurements are considered highly suspect.

Data from the sodar became suspect at higher altitudes, particularly above 400 m.

Data from the total hemispherical radiometer can become corrupted in the early morning due to condensation on the windshield of the sensor. The ventilator attached to the sensor helps reduce the occurrence of this problem. However, during mornings of heavy dew formation, condensation can still occur on the instrument.

Lidar crosswind profiles may tend to smooth out low–level jets or other very non–linear shears (verified by sending simulated wind conditions into a model of the cw lidar and running the same crosswind profiling algorithms). Each lidar observation contains returns from scatterers several range gates from the point of focus. If the wind profile is asymmetric about the point of focus, the lidar wind profile smooths out this asymmetry. Note that measurements in a region of linear vertical shear would not be compromised. The smoothing in the vertical is negligible at low altitudes and becomes more prominent at high altitudes where the lidar beam line–of–sight is much more vertical.

4.3. AVOSS Wind Analysis System (AWAS)

The DFW system is designed with redundant wind data collection systems. They make measurements at similar altitude ranges, but at different places, with different update rates, and with different averaging intervals. Figure 16 shows the altitude range over which quality data can be anticipated from the various wind sensors at DFW. The AVOSS vortex behavior algorithm expects to receive a single profile of horizontal wind, temperature, and turbulence for every time that it runs. Since the redundant wind sensors rarely agree completely with one another, an algorithm was developed to data fuse the wind information into a single profile that characterizes the wind mean and variability. The technology for this algorithm was adapted from the FAA Integrated Terminal Weather System Terminal Winds algorithm (Cole and Wilson, 1994).

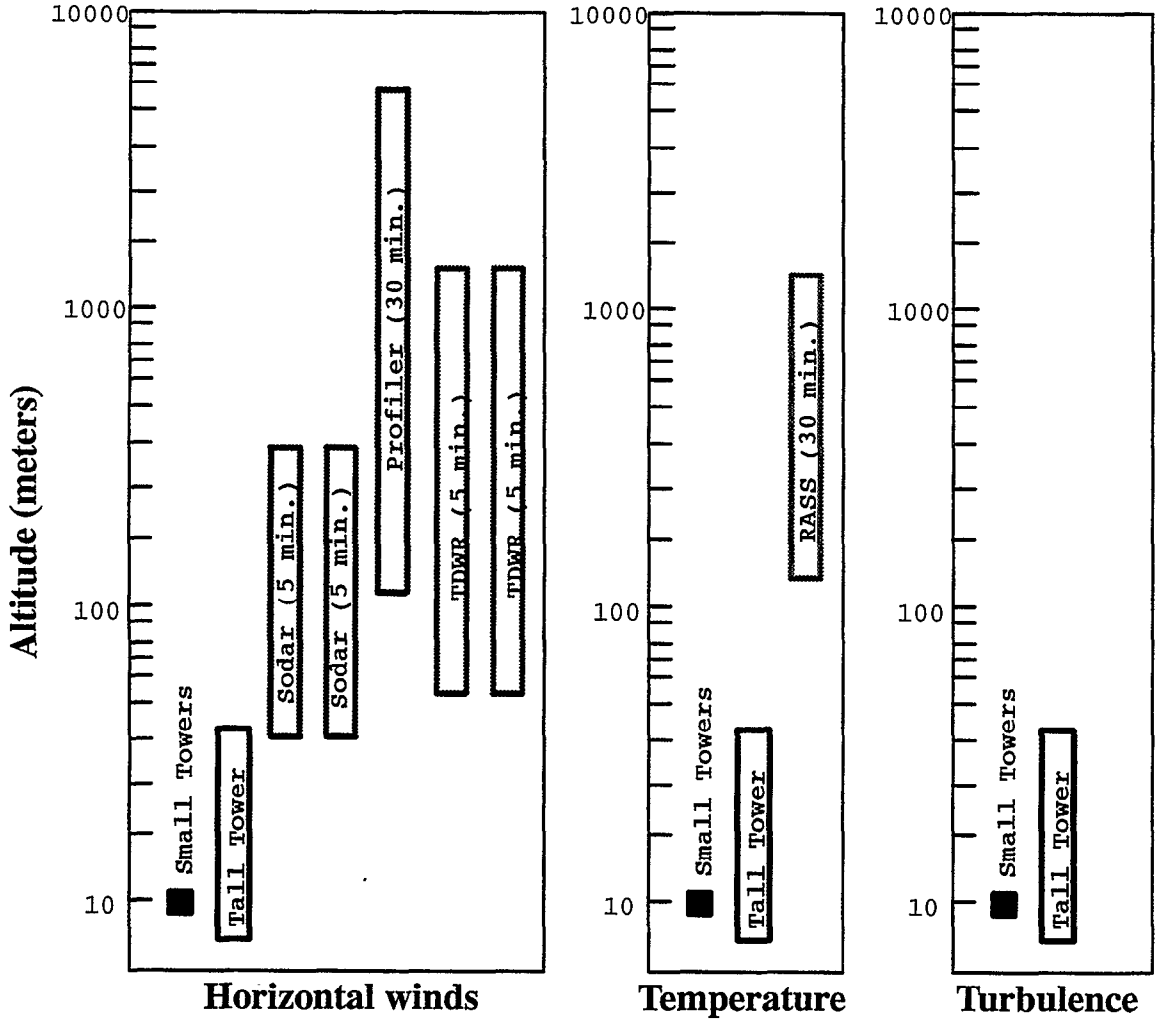

Figure 16. Coverage of the meteorological sensors available in DFW for wind, temperature and turbulence measurements. The time periods show the update rates of the sensors as they were parameterized during the deployment. The update rate is equal to the averaging period, except for the RASS (five-minute average) and the profiler (25-minute average).

4.3.1. Algorithm Design

The requirements for the AVOSS Winds Analysis System (AWAS) are as follows:

- For each operational runway, the system will produce a profile of the following variables:
  - mean headwind
  - headwind error variance
  - mean crosswind
  - crosswind error variance
  - shear of crosswind with altitude
- Each profile will provide these estimates from the ground up to 1400 m AGL.
- Each profile will have vertical resolution of 15 meters to 60 meters, and 50 meters from 100 meters to 1400 meters.

- Each estimate will represent a regional average (nominally equivalent to a 15–minute running average).

Figure 17 provides a high–level overview of the process flow and the primary data flow for the

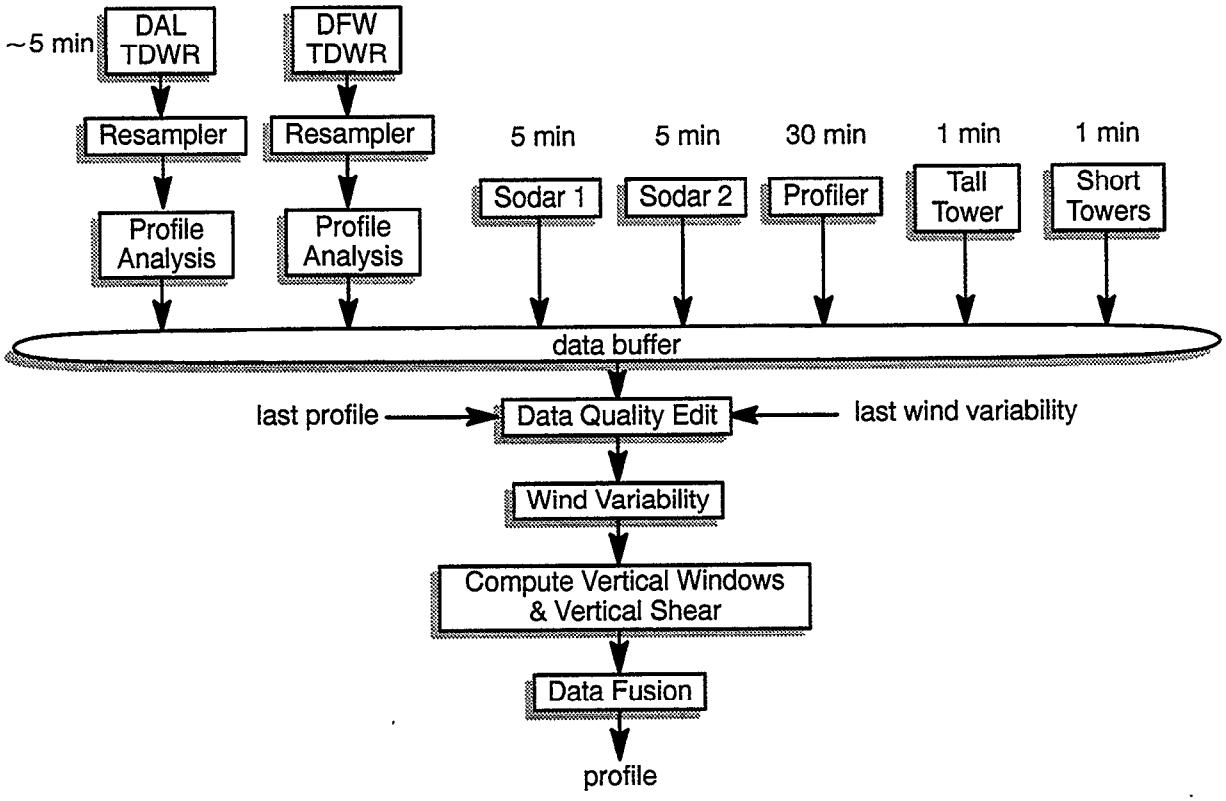

Figure 17. Process flow and primary data flow for the AVOSS winds analysis system.

AWAS. The various sensors are shown across the top, along with their update rates. The Doppler data are processed to construct profiles of mean wind, error variance of the mean wind, and wind field variability. The wind information from the Doppler processing, along with the wind information from the other sensors, feed into a data buffer. The data buffer holds all the information for the previous 15 minutes. Data from the buffer collectively feed into the remaining processing functions every five minutes. The processing modules depicted in Figure 17 are:

1. Resampler: The resampler processes the radial wind components measured by a Doppler radar. Each resampler takes in data from a collection of tilts from a single radar. The data are smoothed using a median filter to remove outliers. Additional data quality editing takes place to remove ground clutter contamination. Finally, the data are resampled onto a Cartesian grid. The current resolution of the resampler output is 2 km.

2. Doppler Profile Analysis (DPA): The DPA takes in a set of wind component estimates from a single resampler (as described in Section 4.2.5.) and produces a profile of estimates of the horizontal winds, estimates of the error variances for the wind estimates, and estimates of the wind field variability. The estimates of headwind and crosswind are extracted from the radial wind components using the Gauss–Markov approach described

below, as are the estimates of the error variances. The wind field variability estimates are computed by comparing the radar measured radial velocities to the corresponding radial component of the estimated mean wind. The size of the region over which data are collected varies between 10 km and 30 km, depending on profile altitude, when data are plentiful. When data are sparse, the window sizes can grow to a maximum of twice as large. At a range of 10 km from the radar, the beam width for a TDWR radar is 87 m. The beam width scales linearly with distance from the radar. However, the effective resolution of the profile is better than the beam width of the most distant data since the data nearer the radar are more heavily weighted. The DPA is only run at a given altitude if there are at least a minimum number of observations on that level, nominally 30 observations.

3. Data quality edit: The data quality edit module removes statistical outliers from the data set. The editing thresholds used are based on expected sensor errors and the previous estimates of wind field variability.
4. Wind variability: The wind variability module takes in the various wind measurements and estimates the variation of the wind about the mean wind by simply computing the root mean square (RMS) difference between the various measured winds and the wind profile.
5. Compute vertical windows and vertical shear: The compute vertical windows module computes the vertical extent of the data window to use for each analysis level. A by–product of this is the vertical shear in the wind. At each analysis level, the data values in a vertical window are examined to see if they exhibit nearly linear shear by fitting a line to the data and checking the resulting fit to the data. The window is increased from a minimum to a maximum extent to find the largest extent over which the data show a linear shear. This extent is then the vertical window used for the given analysis level, and the slope of the associated line is the shear.
6. Data fusion: The data fusion module is based on the the Gauss–Markov implementation described below.

There are two types of errors that affect the use of the estimates of the mean wind by AVOSS. The first is the error in the estimate of the mean wind, and the second is the actual variability of the wind about the mean. The measure of the total error variance as reported by the AWAS is the square root of the sum of the error variance in the reported mean wind and the variance of the wind about the mean wind.

4.3.2. Gauss–Markov Theorem

The AVOSS Wind Analysis System utilizes data from a number of sensors. These sensors provide information of different type, vector or single component, of different scale, and of different quality. To account for these differences, a statistical technique (the Gauss–Markov Theorem) is used to compute the profile of wind values. In order to apply the Gauss–Markov Theorem, the problem must be posed in the form

$$Ax = d, \tag{4}$$

where $x = (u, v)$ is the unknown horizontal wind vector and d contains the observations to be used to estimate the wind vector. The problem is posed and solved independently at each profile level. The

form of the matrix A depends on the type of data, vector and/or radial, to be analyzed. The Gauss–Markov Theorem states that the linear minimum variance unbiased estimate of (u, v) is given by

$$(u, v) = (A^T C^{-1} A)^{-1} A^T C^{-1} \boldsymbol{d}, \tag{5}$$

if each element of $\boldsymbol{d}$ is unbiased and if C is the error covariance matrix for the elements of $\boldsymbol{d}$. The error covariance of the solution is

$$(A^T C^{-1} A)^{-1}. \tag{6}$$

This error covariance is an estimate of the quality of the wind estimate as an estimate of the mean wind; it is not an estimate of the variability in the winds.

When the data for a given profile level contain m vector observations and n Doppler observations, equation (4) has the form:

$$\begin{bmatrix} 1 & 0 \\ 0 & 1 \\ \vdots & \vdots \\ 1 & 0 \\ 0 & 1 \\ \cos\theta_1 & \sin\theta_1 \\ \vdots & \vdots \\ \cos\theta_n & \sin\theta_n \end{bmatrix} \begin{pmatrix} u \\ v \end{pmatrix} = \begin{bmatrix} u_1 \\ v_1 \\ \vdots \\ u_m \\ v_m \\ r_1 \\ \vdots \\ r_n \end{bmatrix}$$

In the DPA, there is always exactly one wind vector observation, the output of the previous DPA run, and the remaining observations are radial. In the data fusion step there are only wind vector observations.

In practice, the error covariance matrix C is not known and must be estimated. The error covariance matrix contains the information that leads to the weights used in averaging the data values to get the optimum fit to the data. There are two types of errors to estimate. The first is the error that arises from an imperfect sensor. The second is the error that arises from the displacement of the sensor from the profile location (displacement error). The error covariance matrix C decomposes into the sum of a sensor error covariance matrix and a displacement error covariance matrix. The sensor error covariance matrix is diagonal.

The displacement error variance models are linear functions of the displacements, horizontal, vertical, and temporal, between the observation location and the analysis location. The displacement error correlation model for two like components is a decreasing exponential function of the displacement between two observation locations. The displacement error covariance model for two non–orthogonal, non–parallel components must take into account the angle between the two components. We denote the angle between the observed component and the u axis by θ, with east at 0° and north at 90°, and the displacement error in observation j by δ_j. Then the displacement error covariance for two observations is given by the following equation:

$$\mathrm{Cov}(\delta_1,\delta_2) = \cos(\theta_1-\theta_2)[\mathrm{Var}(\delta_1)\mathrm{Var}(\delta_2)]^{1/2}\mathrm{Cor}(\delta_1,\delta_2)$$

4.3.3. Selected Results

Figure 18 and Figure 19 show examples of the AWAS data and profiles on two days. Separate profiles for the u and v wind components (east or crosswind, and north or headwind, resp.) are given. The DPA profiles are shown as x and + (DFW and DAL, resp.). The profiler is shown as a diamond, and the sodars are shown as Δ and □ and extend only to 400 m. The tower data appear as a smear at the bottom of the profiles. The large error bars above 1200 m in Figure 18 indicate that there are insufficient data to compute the wind field variability. In Figure 18, all the measurements are in good general agreement, although between 500 m and 1000 m the profiler values show a slightly smaller u component than the DPA profiles. In Figure 18 the output profile has good resolution, capturing the inflection in the u component around 400 m AGL. In Figure 19, the measurements are not in

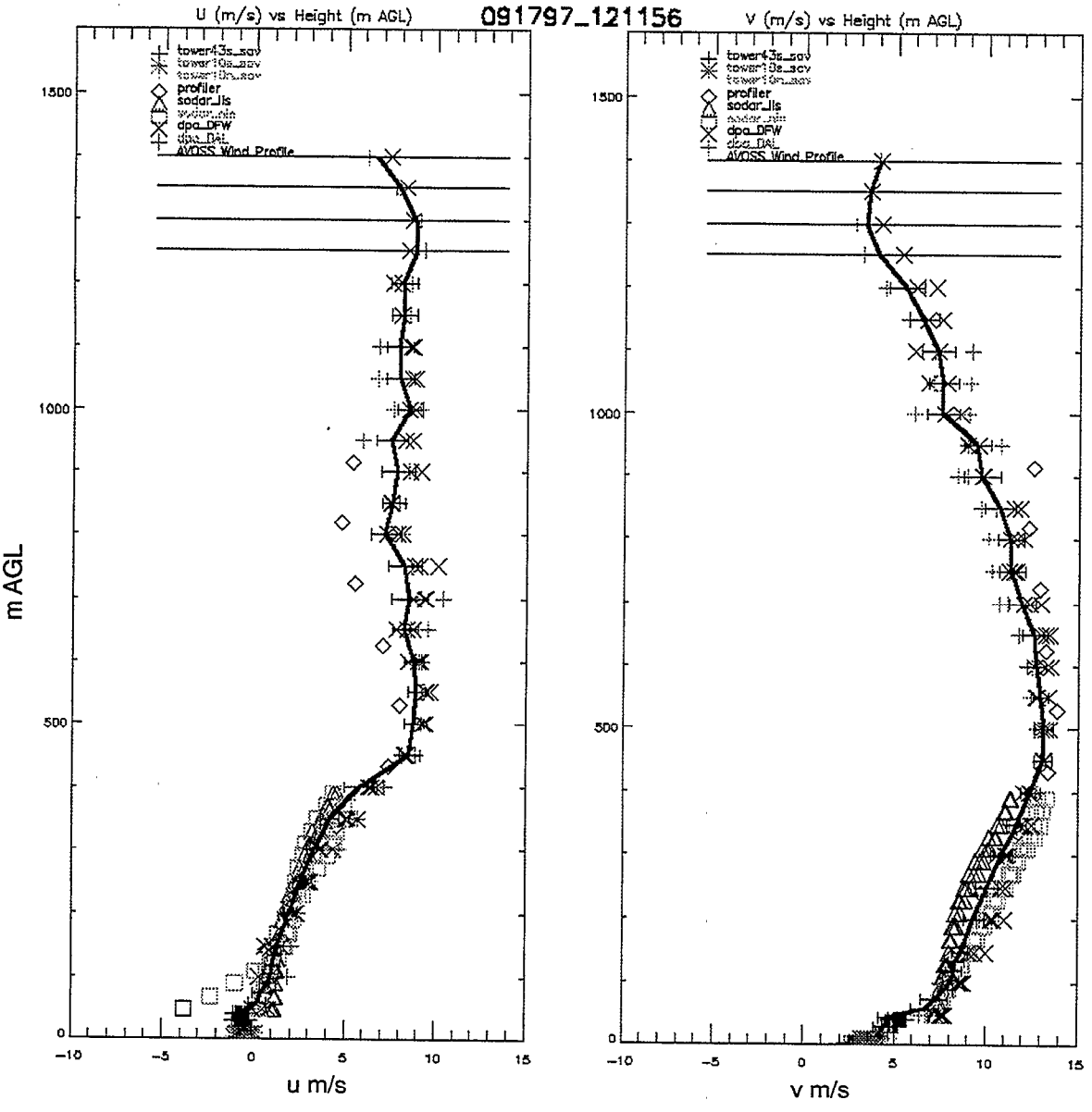

Figure 18. Measurements and the AWAS profile on Sep. 17, 1997 just before 12:12Z.

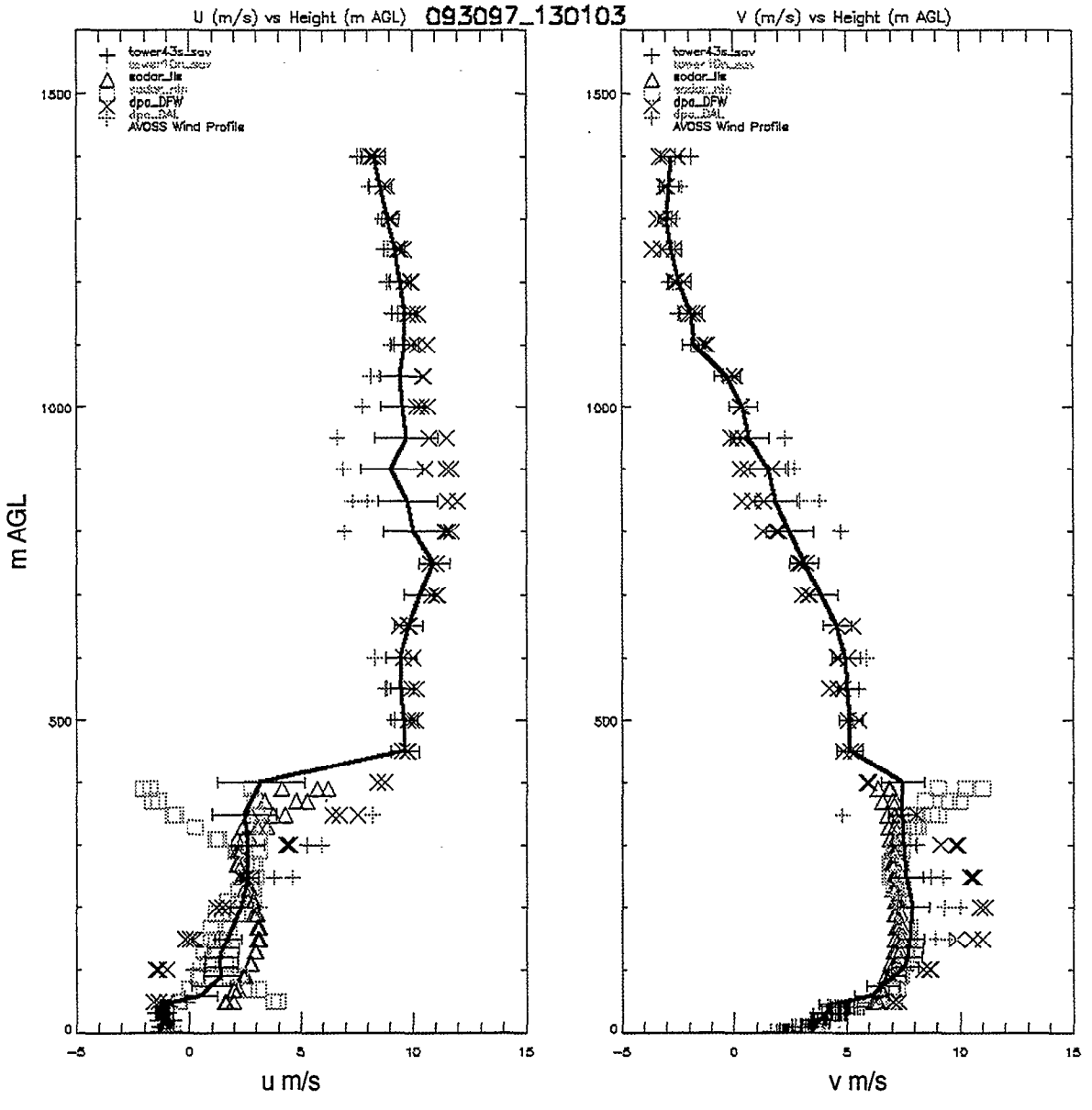

Figure 19. Measurements and the AWAS profile on Sep. 30, 1997 just after 13:01Z.

good general agreement. Cases such as this where there is sensor disagreement need to be examined carefully in light of the particular sensor characteristics. This example shows the need for an improved data quality editing algorithm.

4.3.4. Known Deficiencies

There are a few known deficiencies in the AWAS profiles. Occasionally a profile will have slightly more shear than it should just above the tower height. This is due to the fact that the total weight given the tower data are influenced by how numerous these data are. When the profiler and DPA data are not in general agreement aloft, the profile tends to vary, being closer to the DPA at one altitude and closer to the profiler at the next altitude. This is due to 100 m spacing of the profiler data. One altitude

has a profiler measurement right at that altitude, so that measurement gets a large weight. Also, typically the next higher and lower profiler values are used, giving three profiler values for that altitude. At the next altitude there is no profiler value, so only the next higher and lower profiler values are used, giving only two profiler values used in the AWAS profile at that altitude. This causes the profile to be closer to the DPA values. The last deficiency is in the data quality editing. Occasionally the data quality editing process removes a data value at one altitude, but not similar data values at nearby altitudes. This results in a profile that tends to zig–zag, much like described in the previous problem. This also results in error bars that are larger or smaller than for adjacent altitudes.

5. AIRCRAFT DATA COLLECTION AND PROCESSING

Aircraft data were obtained from the Air Traffic Control (ATC) system. This data consisted of aircraft position and identity from the secondary radar of the Airport Surveillance Radar (ASR–9) and aircraft type from the flight plans filed by the airlines.

The ASR–9 secondary radar (also referred to as the Air Traffic Control Radar Beacon System) provides the identity, altitude, range and azimuth of aircraft with functional transponders. An interrogator antenna on the radar queries each aircraft. The aircraft transponder then transmits back to the radar a unique code identifier and the aircraft altitude. The aircraft position in the horizontal plane is found by determining the range and azimuth of the aircraft.

The flight plan data are received, one per aircraft, approximately one–half hour prior to the aircraft entering the terminal airspace. Each data record contains information on the transponder code, the flight id, the aircraft type, and the coordinated time of arrival at a fix (point in space). The flight ID consists of the airline and flight number for the scheduled airlines, or the tail number of all general aviation aircraft. The transponder code in the flight plan can be matched with the transponder code in the beacon data to associate every aircraft in the terminal area with the type and flight ID.

The radar and flight plan data are processed to determine the time of aircraft passage past a series of AVOSS analysis windows (which include the wake sensor measurement planes), the ground speed, true air speed, descent rate, heading, and position with respect to the runway. Wind data from the meteorological processing are combined with the ground speed to determine the airspeed of the generating aircraft.

The algorithm begins by filtering the input radar data by simply looking at all of the input data for each aircraft as it traverses the analysis window and determining if the radar report is within some distance of the analysis windows. It also looks at the altitude to ensure that the aircraft is at an altitude appropriate for a landing or departing aircraft.

The algorithm then smooths the data about the lidar location using a regression line of 60 seconds worth of radar flight track data. This smoothing is acceptable when the aircraft is on a straight flight path with a constant descent rate. Since the majority of aircraft passing over the lidar are on final approach, they will be maintaining a constant track and glide slope.

The algorithm then determines the aircraft descent rate, ground speed, and heading by using the slope of the regression line. The position relative to the runway is also computed from the regression line using the known location of the analysis window relative to the runway. Finally, the true air speed is computed using the ground speed of the aircraft and the headwind component of the wind estimated from the 42–meter tower wind sensor.

Additional data on landing and takeoff weights were obtained from American Airlines. This data can then be correlated with the other aircraft parameters obtained from the ATC data.

6. MEASUREMENTS

6.1. Vortex Measurements

Vortex data were collected by the CW lidar on 15 days over a three–week period. A general breakdown of the times of the data collections, the number of aircraft in the collection, and the general weather conditions at the time are shown in Table 3. Figure 20 shows the distribution of vortex tracks by time of day. Only a small fraction of tracks were collected during non–daylight hours, in large part due to the lack of traffic on runway 17C/35C during those times. Figure 21 clearly shows that the MD80 family of aircraft was the majority of tracks collected with the CW lidar, although a substantial fraction of the tracks (22 percent) were collected from B757 or heavy aircraft.

Table 3.
Summary of Vortex Data Collected by the Lincoln CW Lidar

Start Date	Time (GMT)	Location	Generation Altitude (meters)	Aircraft	Weather	Winds
9/17/97	1449–1719	17C007	60–80	13	Ptly cldy	S 12 kts
9/18/97	2252–0213	17C007	60–80	17	Clear	SSE 15–20 kts
9/19/97	2230–0218	17C007	60–80	46	Clear	S 12–14 kts
9/21/97	1728–1954	35C007	80–100	37	Ptly cldy	NNE 7–10 kts
9/21/97	2151–2358	35C007	80–100	12	Ptly cldy	ENE 7kts
9/22/97	2016–2331	17C007	60–100	20	Rain/Haze	E–SE 10–20 kts
9/23/97	2244–0052	35CIGE	10–30	7	Cldy (IMC)	NW 14kts
9/24/97	1548–1701	35CIGE	10–30	4	Shower (IMC)	NW 15kts
9/24/97	1941–0014	35CIGE	10–30	27	Cloudy (IMC)	N 15kts
9/25/97	1606–1950	35CIGE	10–30	23	Cloudy (IMC)	N 9–13 kts
9/25/97	2300–0144	35CIGE	10–30	11	Ptly cldy	N 8kts
9/26/97	1624–1729	35CIGE	10–30	15	Ptly cldy	Light & var
9/26/97	1925–2031	35CIGE	10–30	15	Ptly cldy	Light & var
9/28/97	1848–1920	35C007	70–110	4	Clear	N 7kts
9/29/97	1259–1511	35C007	70–110	46	Clear	NE 7kts
9/30/97	1158–2053	17C008	80–110	129	Ptly cldy	S 5kts
10/01/97	1155–2045	17C008	80–110	57	T–storms/ptly cldy	SE–E 10kts
10/02/97	1202–1943	17C008	80–110	116	Ptly cldy	S 8kts
10/03/97	1142–1714	17C008	80–110	91	Clear	S 10–20 kts
			Total Aircraft	**690**		

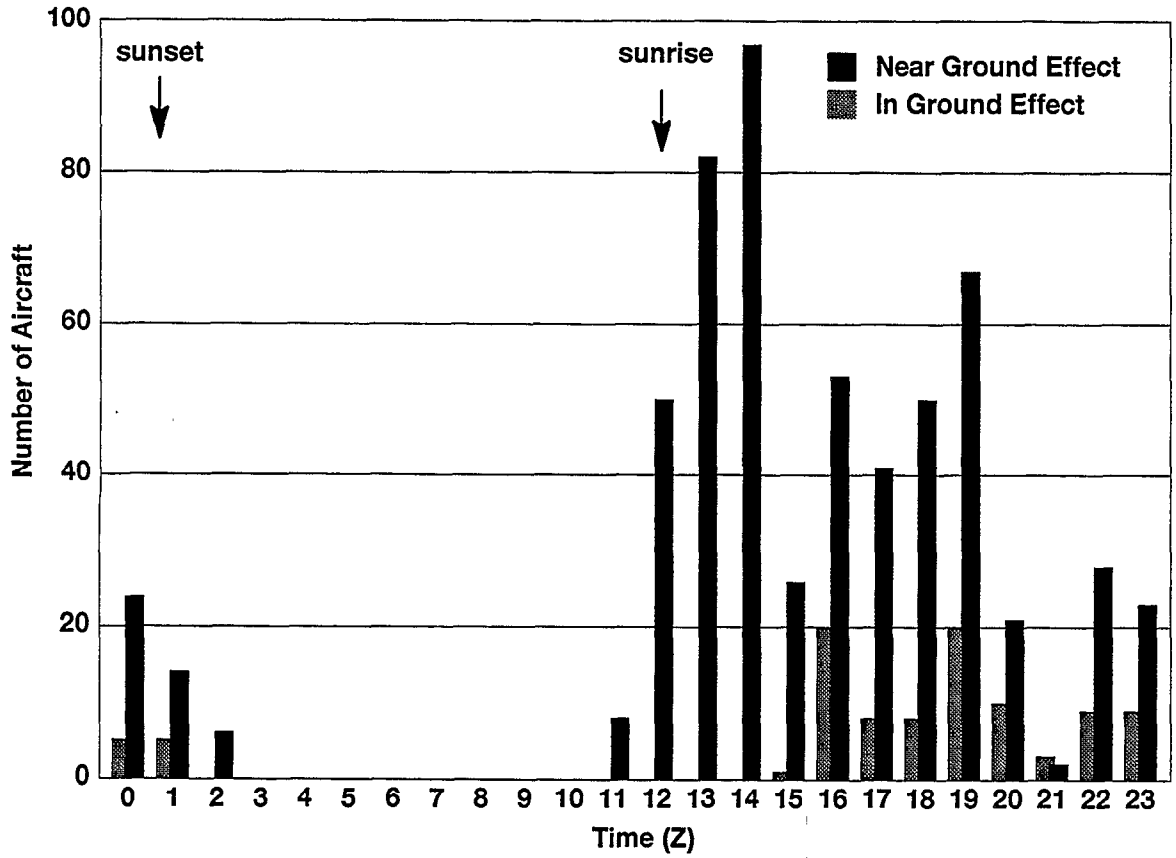

Figure 20. Aircraft vortex data collected by the CW lidar by time of day.

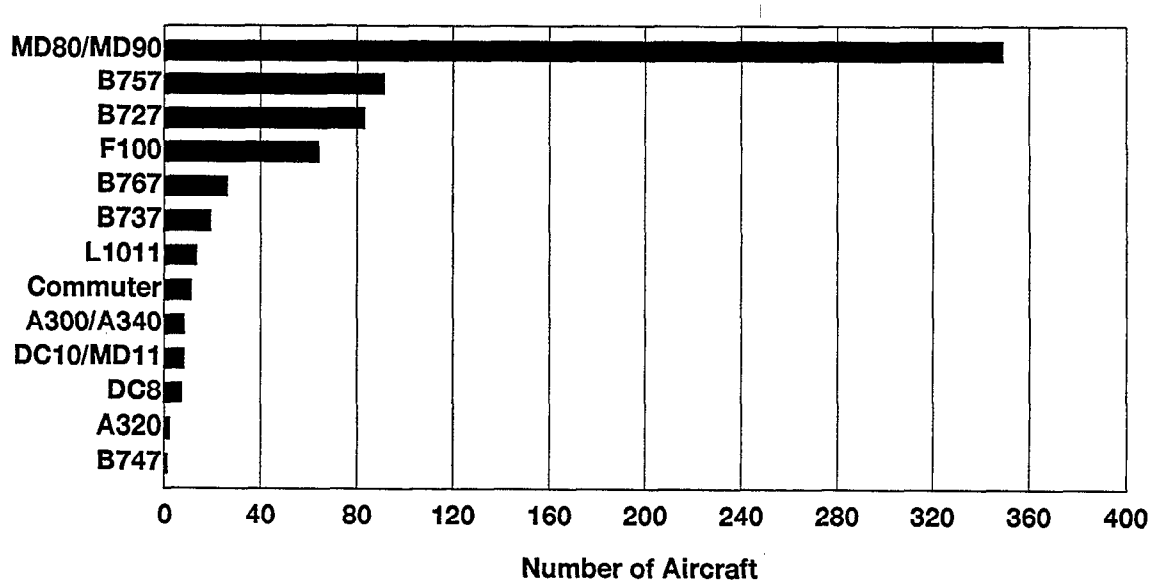

Figure 21. Aircraft vortex data collected by the CW lidar by aircraft type.

6.2. Weather Conditions

During the course of the three–week DFW field deployment, the weather seemed to follow weekly patterns. The first week featured typical summertime conditions with very few clouds, very warm temperatures, high humidity, and winds predominantly out of a southerly direction. The second week was much cooler, with winds mostly out of the north and overcast skies which yielded occasional light precipitation. The final week of the deployment saw conditions revert back to typical summertime conditions, with high heat, humidity, and scattered thunderstorms. The following is a summary of significant meteorological conditions during each lidar collection time for which vortex data were gathered. The turbulent kinetic energy (TKE) values are derived from tower sonic anemometers and represent turbulence estimates over a one–minute averaging period.

970917 – 14:49Z–17:20Z – 17C007

Hot with scattered clouds at 10,000 ft. Winds were out of the south at 12 kts. The atmosphere was neutral to slightly unstable below 100 m during the lidar collection. TKE values were moderately high, with readings from 0.2 – 0.8 m^2/s^2.

970918 – 22:52Z–02:13Z – 17C007

Sunny and hot with gusty southerly winds up to 20 kts. The boundary layer was near neutral and TKE values were high, with average readings of 0.8 m^2/s^2.

970919 – 22:31Z–02:16Z – 17C007

Very hot with scattered clouds at 7000 ft. Winds were southerly at 12–14 kts at the start of the collection period, then shifted to the southeast and slackened to 7 kts by the end of the period. TKE values were moderately high at 0.4–0.8 m^2/s^2. The atmosphere was unstable below 150 m.

970921 – 17:41Z–19:54Z and 21:51Z–23:21Z– 35C007

Cooler with scattered high clouds at 25,000 ft. Winds were out of the north northeast at 7–10 kts. Winds were gusty before the collection period, causing some of the highest TKE values of the deployment (1.5–3.0 m^2/s^2), but by the afternoon readings settled to 0.6–0.8 m^2/s^2.

970922 – 20:38Z–23:31Z – 17C007

Mostly cloudy with overcast at 14,000 ft. and periods of light rain. However, conditions did not meet instrument meteorological conditions (IMC) criteria due to reasonable visibilities and high ceilings. Winds shifted from the east to southeast and gusted up to 20 kts, causing TKE values that approached 1.0 m^2/s^2. The boundary layer was near neutral.

970923 – 22:47Z–00:53Z – 35C IGE

A low overcast ceiling caused IMC conditions during the collection period, but there was no precipitation. Winds were brisk out of the northwest at 14 kts and temperatures were cool. The boundary layer was neutral with very little directional shear with height due to a strong pressure gradient. TKE values were about 0.6 m^2/s^2.

970924 – 15:48Z–18:06Z – 35CIGE

Another IMC day with cloud ceilings from 1200 – 2000 ft. A brief shower occurred during the collection period. Winds were steady out of the NW at 15 kts, with gusts up to 22 kts. TKE values were rather high, averaging around 0.8 with peak readings of 2.0 m^2/s^2.

970924 – 19:49Z–00:07Z – 35CIGE

Similar conditions to the previous collection period earlier in the day. IMC conditions prevailed, but the precipitation had left the area. Crosswinds were as high as 15 kts during this time period.

970925 – 16:19Z–19:35Z – 35CIGE

IMC conditions once again, with cloud ceilings down to 2100–3000 ft. Another cool day with winds out of the north ranging from 9–13 kts. Crosswind values were around 8 kts. TKE values were moderate (0.6 $m^2/s^{2)}$ and the boundary layer was near–neutral.

970925 – 23:09Z–01:42Z – 35CIGE

Clearing skies led to the end of IMC conditions. Winds remained out of the north but decreased to 5–8 kts. Crosswinds decreased considerably as well. The boundary layer was unstable below 100 m due to the heating of the sun and the lack of mixing due to the light winds. TKE was 0.5 m^2/s^2.

970926 – 16:29Z–17:13Z and 19:24Z–20:31Z– 35CIGE

Sunny with cool temperatures and very light and variable winds. TKE values were the lowest of the entire deployment (0.2 m^2/s^2 or less). Although there was plenty of solar heating and little mixing, the boundary layer remained near–neutral during the collection period.

970928 – 18:48Z–19:19Z – 35C007

Variable winds with the passage of a cold front, but speeds were light both before and after. TKE values were low (0.2–0.3 m^2/s^2), but increased somewhat after frontal passage. Crosswinds were light but reversed direction during collection period.

970929 – 12:59Z–15:12Z – 35C007

Clear skies with light north to northeast winds at 5–8 kts. TKE values were about 0.3 m^2/s^2.

970930 – 11:58Z–20:53Z – 17C008

Middle–layer cloud ceiling (10,000–15,000 ft.) was present due to altocumulus clouds originating from dissipated thunderstorms in the area but not nearly low enough to cause IMC conditions. Winds were from the south to southwest in the morning then went calm towards the end of the collection period. The boundary layer remained near–neutral, and TKE values were around 0.5 m^2/s^2 in the morning then approached zero as the winds diminished.

971001 – 11:55Z–20:48Z – 17C008

Scattered thunderstorms and occasional rain through the morning hours, then gradual clearing by afternoon. Winds variable in speed and direction due to various outflows from storms in the area. TKE values were also variable but reached a peak of 1.0–1.5 m^2/s^2 during the morning hours.

971002 – 12:02Z–19:43Z – 17C008

Hot temperatures and scattered clouds. The boundary layer was stable in the morning then progressed to neutral stability with solar heating. Winds varied from southeast to southwest with speeds from 5–10 kts. TKE values were low (0.2 m^2/s^2) in the morning then increased towards afternoon to about 0.6 m^2/s^2. Crosswind values were variable during the beginning of the lidar collection period.

971003 – 11:42Z–17:14Z – 17C008

Clear skies once again. Southerly winds of 10 kts gusted to 20 kts towards early afternoon. Some of the highest TKE values of the deployment were experienced during this time. Morning values were 0.2 m^2/s^2 but then averaged 1.0 m^2/s^2 with peak values of 3.0 m^2/s^2. Weak inversion in the morning and shallow instability in the early afternoon in the boundary layer.

7. SUMMARY

An initial system for the collection and processing of wake vortex, atmospheric and aircraft data at DFW Airport was tested during a measurement period in September and October of 1997. Wake vortices from almost 700 aircraft were observed over a period of 16 days while meteorological measurements were being collected at various locations around the airport, primarily at two special–purpose sites constructed for this project. Wake vortices were observed by the Lincoln CW lidar at four different sites around the airport, all of which were at vortex generation altitudes of about 100 m or less. A large number of measurements of wakes generated inside the runway threshold were also made. Data collection and analysis techniques, the wind data fusion algorithm, general conditions present during the data collection, and data formats have been summarized.

APPENDIX A
DATA FORMATS

This appendix provides the data formats and examples of each type of data. Section A.2 provides the summary file formats, Section A.3 provides the lidar data formats, and Section A.4 provides the meteorological data formats. Section A.1 describes the coordinate systems used in the various files.

All time stamps refer to the beginning of the sensor averaging period.

A.1. Coordinate Systems

Data are provided in one of three different coordinate systems: runway axis coordinate system, lidar axis coordinate system, or meteorological coordinate system.

A.1.1. Runway Axis Coordinate System

The origin of the runway axis coordinate system is the end of the runway. For the runway axis coordinate system, the positive x direction is towards the outer marker, while the negative x direction is down the runway. The positive y direction is towards the right (passenger side or starboard side) of the runway, while the negative y direction is towards the left (driver's side or port side) of the runway. The positive z direction is upward. Figure A–1 depicts the runway axis coordinate system.

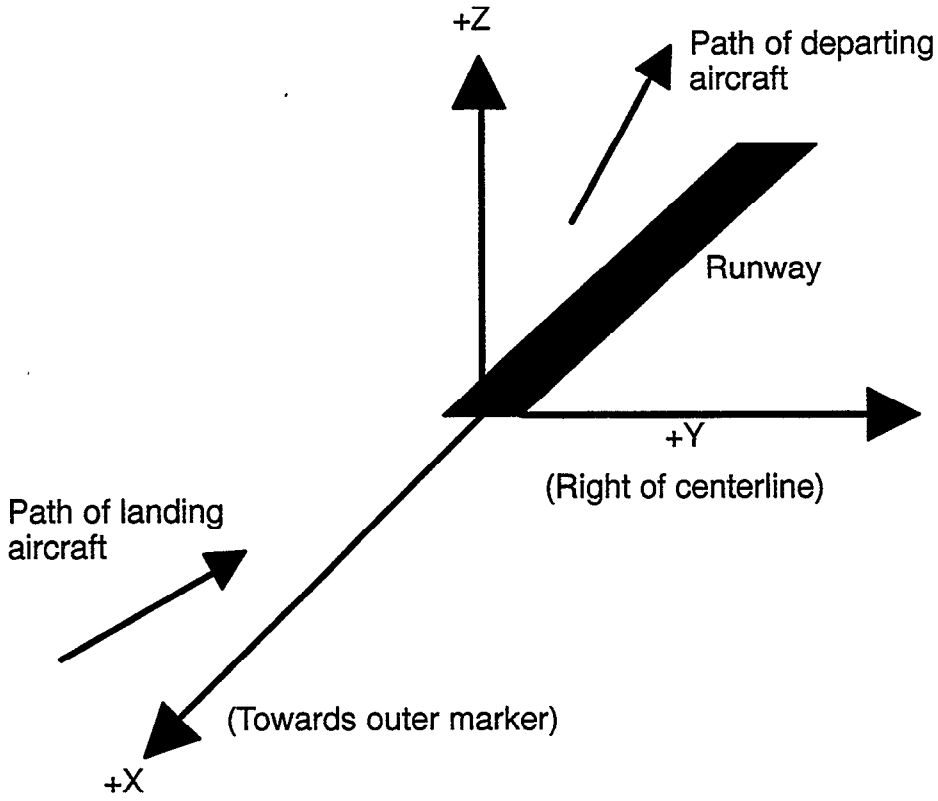

Figure A–1. Runway axis coordinate system.

A.1.2. Lidar Axis Coordinate System

The origin of the lidar axis coordinate system is the ground centered under the scan mirror of the lidar truck. For the lidar axis coordinate system, the positive y direction is to the right (passenger side or starboard side) of the lidar van, while the negative y direction is the the left (driver's side or port side). The positive x direction is toward the rear of the lidar truck, with the negative x direction towards the front of the truck. Finally, the positive z direction is upward. Since the lidar truck is always positioned parallel to the flight path and facing toward the runway, the lidar axis coordinate system matches the runway axis coordinate system, except that the origin is at the lidar truck rather than the runway threshold. Figure A–2 depicts the lidar axis coordinate system.

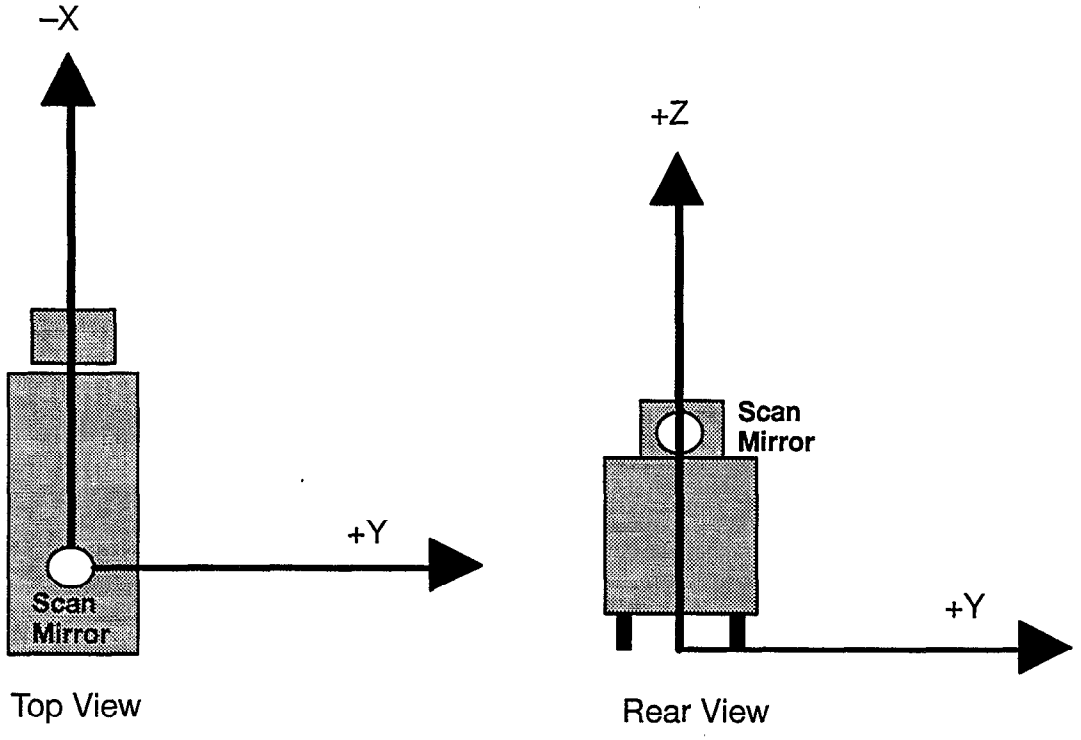

Figure A–2. Lidar axis coordinate system.

A.1.3. Meteorological Axis Coordinate System

The wind data from the meteorological sensors is provided in the meteorological axis coordinate system. For the meteorological axis coordinate system, the origin is the sensor, with the wind direction aligned to true north. The u component of the wind (also known as the east–west wind component) is positive when the wind is blowing from west to east and negative when the wind is blowing from east to west. The v component of the wind (also known as the north–south wind component), is positive when the wind is blowing from south to north and negative from north to south.

A.2. Summary File

The summary file consists of vortex track and aircraft information. Each aircraft event consists of one line of data. This information provides a quick look at the high–level wake vortex data. One

file is produced for the entire data set. The format of the summary file is shown in Table A–1 and is also included as a header to the file. All aircraft position data are provided in the runway axis coordinate system.

Table A–1.
Wake Vortex Summary File Contents

	Parameter	Units	Comments
1	Year	N/A	In GMT time, changes with 2400Z
2	Month	N/A	
3	Day	N/A	
4	Hour	N/A	GMT Time of aircraft passage over the Lidar,
5	Minute	N/A	
6	Second	N/A	
7	Lidar Site Name	N/A	Name of Lidar site at which vortex data was collected
8	Aircraft Type	N/A	From beacon processes, major type, i.e., B727,DC9
9	Aircraft Model	N/A	From airline data, within aircraft type, i.e., 200,300
10	Aircraft Altitude	m	From filtered & smoothed beacon data & barometer setting
11	Aircraft Ground Speed	m/s	From filtered & smoothed beacon data
12	Aircraft True Air Speed	m/s	From filtered & smoothed beacon data & winds data
13	Aircraft Climb Rate	m/s	From filtered & smoothed beacon data & winds data; positive is upward
14	Aircraft Weight	lbs	From airline data.
15	Aircraft Wingspan	m	Diagnosed from the type using manufacturers data.
16	Port track number of points	N/A	Number of position estimates for port vortex track.
17	Port track starting time	s	Seconds since aircraft passage of first port track point.
18	Port track ending time	s	Seconds since aircraft passage of last port track point.
19	Starboard track number of points	N/A	Number of position estimates for starboard vortex track.
20	Starboard track starting time	s	Seconds since aircraft passage of first starboard track point.
21	Starboard track ending time	s	Seconds since aircraft passage of last starboard track point.

A.3. Lidar Data

There are three types of lidar wake data files currently provided: wake vortex circulation and location data, wake vortex velocity profile files, and lidar–generated wind profiles.

A.3.1. Wake Vortex Location and Circulation Estimates

The format for the wake vortex location and circulation estimate data are shown in Table A–2 and Table A–3, the header and data content formats, respectively. This format is identical to the format in which the Memphis data files were provided. Additional aircraft information, such as weight, wingspan and airspeed, is provided as a comment line in a way that does not change the length of the file from the Memphis format (format 02P). All wake vortex location data are provided in the lidar axis coordinate system.

Table A–2.
Wake Location and Circulation File Header Data

Line 1	
Vortex sign	i.e., "Port" or "Starboard"
Airport	i.e., "DFW"
Lidar Site Name	Name of Lidar site at which vortex data was collected
Case Number	Not used for the DFW data. Included for conformity to Memphis Data format.
Aircraft Type	From beacon processes, major type, i.e., B727, DC9
Aircraft model	From airline data, within aircraft type, i.e., 200, 300
Line 2	
Algorithm Version	Version of data processing algorithm used to generate this data set indicated by a number and a following letter. The letter "P" indicates postprocessed data while "R" indicates real–time data.
Data Format	File format number. This document describes the content of file format 4.
Line 3	
Year	Time of aircraft Passage
Month	
Day	
Hour	
Minute	
Seconds	

Table A–3.
Wake Vortex Location and Circulation Estimates Data Format

Relative Time	sec	Time Since Aircraft Passage
Y–position	meters	Estimated distance of center of the vortex core laterally from the center of the lidar truck.
Relative Y–error (dely)	meters	Relative Z–location estimation error using estimates of angle and range estimation errors. Angle estimation error is considered small compared to range estimation error. Range estimation error is given as the half–width of the range optimization cost function. This value should be related to range error but may not be absolutely accurate.
Z–position	meters	Estimated altitude of the center of the vortex core from the ground altitude at the lidar. Transformations to polar coordinates should subtract 3.86 m from this value first, corresponding to the height of the lidar scan mirror above the ground.
Relative Z–error (delz)	meters	Relative Z–location estimation error, using estimates of angle and range estimation errors. Angle estimation error is considered small compared to range estimation error. Range estimation error is given as the half–width of the range optimization cost function. This value should be related to range error but may not be absolutely accurate.
Vortex range deviation from lidar focus (r0)	meters	Lidar focus range – vortex range. May be useful in understanding how well focused the lidar was on the vortex for this scan. Vortices closer in focus may lead to more reliable tangential velocity estimates, particularly nearer to the vortex core.
Maximum and minimum velocity cross–range distance	meters	Cross–range distance between the most positive detectable vortex velocity and the most negative detectable vortex velocity. Should be an upper bound on the vortex core diameter from this viewing angle.
Vortex average circulations { gamma(–25), ..., gamma(25) }	m^2/sec	Average circulation estimates of the vortex, at one meter increments from the vortex core, out to 25 meters in each direction. All measurement points within 0.5 m of each estimate point are used in the averaging.

A.3.2. Wake Vortex Tangential Velocity Profiles

The format for the wake vortex velocity profile data are shown in Table A–4. There are three lines in the file preceding that indicated in Table A–4, but these lines have identical content to that described in Table A–2. All wake vortex location data are provided in the lidar axis coordinate system.

Table A–4.
LIDAR Wake Velocity Profiles

Line 1		
Number of tangential velocity profile points	unitless	Indicates number of lines that will follow this one with velocity estimates.
Relative time	sec	Seconds since aircraft passage.
Y–position	meters	Estimated distance of center of the vortex core laterally from the center of the lidar truck.
Relative Y–error	meters	Relative Z–location estimation error using estimates of angle and range estimation errors. Angle estimation error is considered small compared to range estimation error. Range estimation error is given as the half–width of the range optimization cost function. This value should be related to range error but may not be absolutely accurate.
Z–position	meters	Estimated altitude of the center of the vortex core from the ground altitude at the lidar. Transformations to polar coordinates should subtract 3.86 m from this value first, corresponding to the height of the lidar scan mirror above the ground.
Relative Z–error	meters	Relative Z–location estimation error, using estimates of angle and range estimation errors. Angle estimation error is considered small compared to range estimation error. Range estimation error is given as the half–width of the range optimization cost function. This value should be related to range error, but may not be absolutely accurate.
Focus Range	meters	Lidar focus range from lidar.
Vortex Range	meters	Vortex range from lidar.
Lines 2–n		
Cross–range distance	meters	Distance in direction perpendicular to the lidar line–of–sight from the vortex core.
Tangential Velocity	m/s	Modified Maximum velocity estimate at this cross–range distance.

A.3.3. Lidar Wind Measurements

Table A–5 details the contents of the lidar wind profile files. Only the crosswind component was estimated by the CW lidar. The files repeat the data structure shown in Table A–5 until all averaging periods are detailed. All lidar crosswind data are provided in the lidar axis coordinate system.

Table A–5.
Lidar Crosswind File Data

Line 1	
AVOSS window ID	Text identifier of AVOSS window location.
Receive time	GMT time real–time system received the wind profile.
Date	GMT date of beginning of averaging period.
Start time	GMT time of beginning of averaging period.
Latitude	Wind profile reference latitude.
Longitude	Wind profile reference longitude.
Runway	Runway lidar sensor was using to monitor arrival aircraft.
Ground Altitude	Wind profile ground altitude above sea level (m)
Averaging Period	Length of averaging period (s).
Line 2	Comment Line
Line 3	Number of profile levels (n)
Line 4 – (4+n)	
Height	Profile level height above ground.
Wind speed	Magnitude of wind.
Wind Direction	Direction of wind.
X component	Mean headwind/tailwind component.
Y component	Mean crosswind component.
X–component variance	Variance of headwind/tailwind component.
Y–component variance	Variance of crosswind component.
Repeat above block to EOF	

A.4. Meteorological Data

A number of different data file formats have been defined for distribution of the meteorological data files to NASA. These consist of the SAVPAK data files, the FLUXPAK data files, the Soil data files, the Doppler Profile Analysis (DPA) files, and the Atmospheric Profile files. Each data file format is specified below. All meteorological data are provided in the meteorological axis coordinate system.

The SAVPAK data files consist of the standard atmospheric variables measured by the five sensor packages located on the instrumented towers. The sensors directly measure the ambient temperature, relative humidity, wind speed and direction. The software included in the savpak_server computes the virtual temperature, potential temperature, virtual potential temperature, and north–south, east–west wind components. The pressure is measured at the actual barometer locations and estimated

for the SAVPAK locations. All data are one–minute averages output every minute. The SAVPAK data format is shown in Table A–6.

The FLUXPAK data files consist of the covariance measurements at the sonic anemometer locations on the instrumented towers. The sensors directly measure the east–west and north–south wind component as well as the virtual temperature. All measurements are performed at a 10Hz data rate, averaged for one minute and output every minute. The format for the FLUXPAK data are shown in Table A–7.

The Soil data files consist of the soil measurements performed at both the north and south meteorological sites. The sensors' output included in this data file are the Soil Temperature Probe (STP–1), the Soil Moisture Probe (SMP–1), the Rain Gauge (TE525), and the Total Hemispherical Radiometer (THRDS–7). The Soil Temperature Probe and the Soil Moisture Probe are located at the depth indicated in the file. The Rain Gauge and Radiometer are mounted on an aluminium structure at a two–meter height. All data are one–minute averages output every minute. The Soil data file format is shown in Table A–8.

The Doppler Profile Analysis (DPA) files contain wind profile information derived from TDWR data. A file is created for each GMT calendar day for each TDWR radar and is separated internally into five–minute blocks. Each block contains a commented header (comment lines are denoted by a # symbol as the first character). Each header is followed by the actual wind data provided by the DPA algorithm. The DPA file format is shown in Table A–9 and Table A–10.

The wind profile data files contain headwind and crosswind information provided by the AVOSS Wind Analysis System (AWAS). A file is created for each GMT calendar day and is separated internally by five–minute blocks. Each block contains a commented header (comment lines are denoted by a # symbol as the first character). Each header is followed by the actual headwind and crosswind data. The AWAS file format is shown in Table A–11 and Table A–12.

Table A–6.
SAVPAK Data File Contents

	Variable	Units	Description
1	Year		Date of data collection, changes with 2400Z
2	Month		
3	Day		
4	Hour		Start time of data collection
5	Minute		
6	Seconds		
7	Height	meters AGL	Height of sensor package above ground level
8	Pressure	Millibars	Pressure at sensor package height, estimated from 2–meter barometer, using Standard Atmospheric Assumption
9	Ambient Temperature	degrees C	Ambient Temperature, from R.M. Young Temperature/Relative Humidity Probe
10	Virtual Temperature	degrees C	Virtual Temperature, computed from Temperature, Dew Point, and Pressure
11	Potential Temperature	degrees K	Potential Temperature, computed from Temperature and Pressure
12	Virtual Potential Temperature	degrees K	Virtual Potential Temperature, computed from Virtual Temperature, and Pressure
13	Dew Point	degrees C	Dew Point, computed from Ambient Temperature and Relative Humidity
14	Relative Humidity	%	Relative Humidity, from R.M. Young Temperature/Relative Humidity Probe
15	Wind Speed	m/s	Wind Speed, from R.M. Young Wind Monitor AQ
16	Wind Direction	degrees	Wind Direction, from R.M. Young Wind Monitor AQ
17	U component	m/s	U Component from Wind Direction and Wind Speed
18	V component	m/s	V Component from Wind Direction and Wind Speed
19	W component	m/s	W Component, not available at current time

Table A–7.
FLUXPAK Data File Contents

	Variable	Units	Description
1	Year	N/A	Date of data collection, changes with 2400Z
2	Month	N/A	
3	Day	N/A	
4	Hour	N/A	Start time of data collection
5	Minute	N/A	
6	Seconds	N/A	
7	Height	meters AGL	Height of sensor package above ground level
	U component	m/s	East–West component of the wind
	V component	m/s	North–South component of the wind
	W component	m/s	Vertical component of the wind
	Virtual Temperature	K	Virtual Temperature as measured by the sonic anemometer
	Mxing Ratio	g/m^3	Mixing Ratio measured by the krypton hygrometer (not available in 97)
	u'u'	m^2/s^2	Covariances
	u'v'	m^2/s^2	
	u'w'	m^2/s^2	
	u't'	Km/s	
	u'q'	g/m^2s	
	v'v'	m^2/s^2	
	v'w'	m^2/s^2	
	v't'	Km/s	Covariances
	v'q'	g/m^2s	
	w'w'	m^2/s^2	
	w't'	Km/s	
	w'q'	g/m^2s	
	t't'	K^2	
	t'q'	Kg/m^3	
	q'q'	g^2/m^6	
12	tke	m^2/s^2	Turbulent Kinetic Energy

Table A–8.
Soil Data File Contents

Line 1	Soil sensor suite text identifier
Line 2	
Latitude	Reference latitude.
Longitude	Reference longitude.
Ground Altitude	Ground altitude above sea level (m)
Line 3	
Year	Date of start of averaging period (Z).
Month	
Day	
Hour	Time of start of averaging period (Z).
Minute	
Second	
Averaging Period	Length of averaging period (s).
Line 4	
Rainfall	Rainfall in averaging period (inches).
Line 5	
Total Hemispherical Radiation Incoming	Incoming Radiation (W/m^2)
Total Hemispherical Radiation Outgoing	Outgoing Radiation (W/m^2)
Net Radiation	Incoming Radiation – Outgoing Radiation (W/m^2)
Line 6–8	
Soil Depth	Depth of soil sensor from ground level (m)
Soil Temperature	Temperature of soil at this depth (degrees C)
Soil Moisture	Percent water content at this depth.
Repeat above block to EOF	

Table A–9.
Doppler Profile Analysis Data Header

Line	Description
Radar identifier	Radar from which data originated
Location	Latitude, longitude, surface altitude (MSL)
Time	Month, day, year, hour, minute, second, number of seconds to complete radar volume scan
Number of levels	Number of interpolated levels in data block

Table A–10.
Doppler Profile Analysis Data File Contents

	Variable	Units	Description
1	Height	meters AGL	Height at which values are interpolated
2	Number of points		Number of 1 km data points in sample
3	Age	seconds	Age of data for each level relative to time stamp
4	Wind speed	m/s	
5	Wind direction	m/s	Oriented from true north
6	U–wind	m/s	East–west wind component
7	V–wind	m/s	North–south wind component
8	U–variance	m/s	Variance in estimate of U–wind
9	V–variance	m/s	Variance in estimate of V–wind
10	RMS1	m/s	Root mean square value using number of points used in estimate
11	RMS2	m/s	Root mean square using all available radar data points

Table A–11.
AWAS Data Header

Data identifier	Identifier for type of data to follow
Profile location	latitude, longitude, reference altitude (MSL)
Time of profile	Month, day, year, hour, minute, second
Rotation from true north	Data orientation
Number of levels	Number of levels in profile data block

Table A–12.
AWAS Data File Contents

	Variable	Units	Description
1	Height	meters AGL	Height at which values are interpolated
2	Crosswind	m/s	Crosswind component
3	Headwind	m/s	Headwind component
4	Crosswind variance	m/s	Goodness of fit for crosswind
5	Headwind variance	m/s	Goodness of fit for headwind
6	Crosswind spatial variability	m/s	Crosswind average of all current sensor variability readings
7	Headwind spatial variability	m/s	Headwind average of all current sensor variability readings
8	Crosswind temporal variability	m/s	Crosswind average of all past crosswind sensor variability readings
9	Headwind temporal variability	m/s	Headwind average of all past crosswind sensor variability readings
10	Crosswind vertical shear	m/s / m	Change in crosswind values with height

APPENDIX B
METEOROLOGICAL SENSOR CHARACTERISTICS

The meteorological data acquisition systems are listed below in Table B–1. The sensor and the parameters that the sensor measures are listed in the first two columns of the table. The next two columns, listed the measurement frequency (Data Collection Frequency) and time–averaging (Averaging Period) of the parameter. The last two columns listed the measurement range of the parameter as well as the measurement accuracy of the parameter. In some cases, this information is obtained from the sensor owner's manual, in other cases the information is obtained from discussions with the manufacturer.

Table B–1.
Meteorological Sensor Characteristics

Sensor	Parameter	Data Collection Frequency	Averaging Period	Range	Accuracy
R.M. Young Temp/RH sensor model 41372C	Temperature	1 Hz	1 min.	±50°C	0.3°C
	Relative Humidity	1 Hz	1 min.	0–100%	2% 0–90% 3% 90–100%
R.M. Young Wind Monitor–AQ model 05305	Wind Speed	1 Hz	1 min.	0.4–40 m/s	2%
	Wind Direction	1 Hz	1 min.	0–360 degrees	3 degrees
Applied Technologies SWS–211/3Sx	Virtual Temperature	10 Hz	1 min.	–20 to 50°C	0.05 °C
	U Component	10 Hz	1 min.	±15 m/s	0.05 m/s
	V Component	10 Hz	1 min.	±15 m/s	0.05 m/s
	W Component	10 Hz	1 min.	±15 m/s	0.05 m/s
Campbell Scientific Krypton Hygrometer KH–20	Mixing Ratio	20 Hz	1 min.	1–20 g/m^3	0.5 g/m^3
Vaisala Barometer PTA427	Pressure	1 Hz	1 min.	800–1100 mb.	0.15 mb.
Radiation Energy Balance Systems Total Hemispherical Radiometer THRDS7	Net Radiation	1 Hz	1 min.	–1000–2000 W/m^2	N/A
	Total Hemispherical Ration Incoming	1 Hz	1 min.	–1000–2000 W/m^2	N/A
	Total Hemispherical Radiation Outgoing	1 Hz	1 min.	–1000–2000 W/m^2	N/A
Radiation Energy Balance Systems Soil Moisture Probe SMP–1	Temperature	1 Hz	1 min.	±50°C	0.05°C

Table B–1.
(Continued)

Sensor	Parameter	Data Collection Frequency	Averaging Period	Range	Accuracy
Radiation Energy Balance Systems Soil Temperature Probe STP–1	Soil Moisture	1 Hz	1 min.	0–35 % Water Content	N/A
Texas Electronics Tipping Bucket Rain Gauge TE525	Rain Rate	0.01"	1 min.	0–2" /hr.	1 %
Radian Corp. LAP3000 (Profiler)	Wind Speed	N/A	25 min.	0–51m/s	1 m/s
	Wind Direction	N/A	25 min.	0–360 degrees	10 degrees
Radian Corp. RASS	Virtual Temperature	N/A	5 min.	±32°C	1°C
Remtech PA2 Sodar	Wind Speed	N/A	5 min.	0–40m/s	0.2 m/s if wind speed < 6m/s otherwise, 3% of wind speed
	Wind Direction	N/A	5 min.	0–360 degrees	5 degrees
	W Component	N/A	5 min.	±4m/s	5 cm/s
LORAN CLASS sounding system	Temperature	2 Hz.	10 sec.	±50°C	1°C
	Relative Humidity	2 Hz.	10 sec.	0–100 %	3 %
	Wind Speed	2 Hz.	60 sec.	0–50 m/s	1 m/s
	Wind Direction	2 Hz.	60 sec.	0–360 degrees	10 degrees
	Pressure	2 Hz.	10 sec.	50–1100 mb	1 mb.

GLOSSARY

AGL	Above Ground Level
ASR–9	Airport Surveillance System 9
ATC	Air Traffic Control
AVOSS	Aircraft Vortex Spacing System
AWAS	AVOSS Wind Analysis System
CTAS	Center TRACON Automation System
CW	Continuous Wave
DFW	Dallas/Ft. Worth International Airport
DPA	Doppler Profile Analysis
DSP	Digital Signal Processing
FAA	Federal Aviation Administration
GMT	Greenwich Mean Time
IFR	Instrument Flight Rules
ITWS	Integrated Terminal Weather System
MEM	Memphis International Airport
MSL	Mean Sea Level
NASA	National Aeronautics and Space Administration
NIST	National Institute of Standards and Technology
RH	Relative Humidity
RMS	Root Mean Square
RTD	Resistance vs. Temperature Device
TKE	Turbulent Kinetic Energy

REFERENCES

Burnham, D.C. "Review of Vortex Sensor Development Since 1970," *Proc. of the Aircraft Wake Vortex Conference*, FAA–RD–77–68, Cambridge, MA, 1977.

Campbell, S.D., Dasey, T. J., Heinrichs, R.M. and M. P. Matthews , "Overview of 1994 Memphis Wake Vortex Testing Program," *Proc. Sixth Conference on Aviation Weather Systems*, American Meteorological Society, Boston, MA, pp. 515–520, 1995.

Campbell, S., Dasey, T., Freehart, R., Heinrichs, R., Matthews, M. and Perras, G., "Wake Vortex Field Measurement Program at Memphis, TN," AIAA Paper No. 96–0399, 1996.

Campbell, S. D., Dasey, T. J., Freehart, R. E., Heinrichs, R. M., Matthews, M. P., Perras, G. H., and G. S. Rowe, "Wake Vortex Field Measurement Program at Memphis, TN Data Guide," Lincoln Laboratory Project Report NASA/L–2, 1997.

Cole, R. E. and F. W. Wilson, "The Integrated Terminal Weather System Terminal Winds Product," *Lincoln Laboratory Journal*, Vol 7, No. 2, 1994.

Constant, G., Foord, R., Forrester, P.A., and J.M. Vaughan, "Coherent Laser Radar and the problem of aircraft wake vortices," *J. Modern Optics*, 41(11), 2153–2173, 1994.

Dasey, T. J., and R. Heinrichs, "An Algorithm for the Recognition and Tracking of Aircraft Wake Vortices with a Continuous Wave Coherent Laser Radar," *Coherent Laser Radar*, Vol. 19, OSA Technical Digest Series (Optical Society of America, Washington, DC), pp. 193–196, 1995.

Dasey, T. J., Campbell, S. D., Heinrichs, R. M., Matthews, M. P., Freehart, R. E., Perras, G. P., and P. Salamitou, "A Comprehensive System for Measuring Wake Vortex Behavior and Related Atmospheric Conditions at Memphis, Tennessee," *Air Traffic Control Quarterly*, 5(1), 49–68, 1997.

Denery, D. G. and H. Erzberger (1995). "The Center–TRACON Automation System: Simulation and Field Testing," Oct. 2–6, Capri, Italy, *Proc. of the Advanced Workshop on ATM* (ATM95), (also NASA Technical Memorandum 110366, August, 1995).

Evans, J. E. and E. R. Ducot, "The Integrated Terminal Weather System (ITWS)," *The Lincoln Laboratory Journal* 7(2): 449–474, 1994.

Heinrichs, R.M, Freehart, R.E., Dasey, T.J. and Mandra, R.S., "Development and Performance of a CW Coherent Laser Radar for Detecting Wake Vortices," *Coherent Laser Radar*, Vol. 19, 1995, OSA Technical Digest Series (Optical Society of America, Washington DC, 1995), 186–189, 1995.

Heinrichs, R.M., Dasey, T.J., Matthews, M.P., Campbell, S.D., Freehart, R.E., Perras, G.H., and P. Salamitou, "Measurements of Aircraft Wake Vortices at Memphis International Airport with a CW CO_2 Coherent Laser Radar," *Proc. SPIE 10th International Aerosense Symposium, Air Traffic Control Technologies II*, Vol. 2737, 122–133, 1996.

Heinrichs, R. M. and T. J. Dasey, "Analysis of Circulation from a Wake Vortex Lidar", AIAA Paper No. 97–0057, 1997.

Hinton, D.A., "Aircraft Vortex Spacing System (AVOSS) Conceptual Design," NASA Technical Memorandum 110184, NASA Langley Research Center, Hampton, VA, 1995.

Huffaker, R.M., Jelalian, A.V. and J.A. Thomson, "Laser Doppler System for Detection of Aircraft Trailing Vortices," *Proc. IEEE*, 58(3), 322–326, 1970.

Koepp, F., "The Infrared Doppler Lidar: An Important Tool for Experimental Investigation of Aircraft Wake Vortices," *Technical Digest on Coherent Laser Radar: Technology and Applications* (Optical Society of America, Washington, DC), 12, 306–308, 1991.

Matthews, M., Dasey, T. J., Perras, G. H. and S. D. Campbel, "Planetary Boundary Layer Measurements for the Understanding of Aircraft Wake Vortex Behavior," *Proc. 7th AMS Conference on Aviation Weather Systems* (American Meteorological Society, Boston, MA,), pp. 175–180, 1997.

Salamitou, P. and R.J. Hansman, "An Algorithm for CW Doppler Lidar Wake Vortex Remote Sensing," *Coherent Laser Radar*, Vol. 19, 1995 OSA Technical Digest Series (Optical Society of America, Washington, DC), PDP 3–2, 1995.

Tardif, R., Beauchemin, M., Zwack, P. and J. L. Keller, "The COBEL Model as Part of a Terminal–Area Ceiling & Visability (C&V) Nowcast System: A Progress Report," Lincoln Laboratory Project Report ATC–241, 1996.

Thompson, S. D., "Terminal Area Separation Standards: Historical Development, Current Standards, and Processes for Change," Lincoln Laboratory Project Report ATC–258, 1997.